iScience

CellPress
OPEN ACCESS

Article

Microbiota-Sourced Purines Support Wound Healing and Mucous Barrier Function

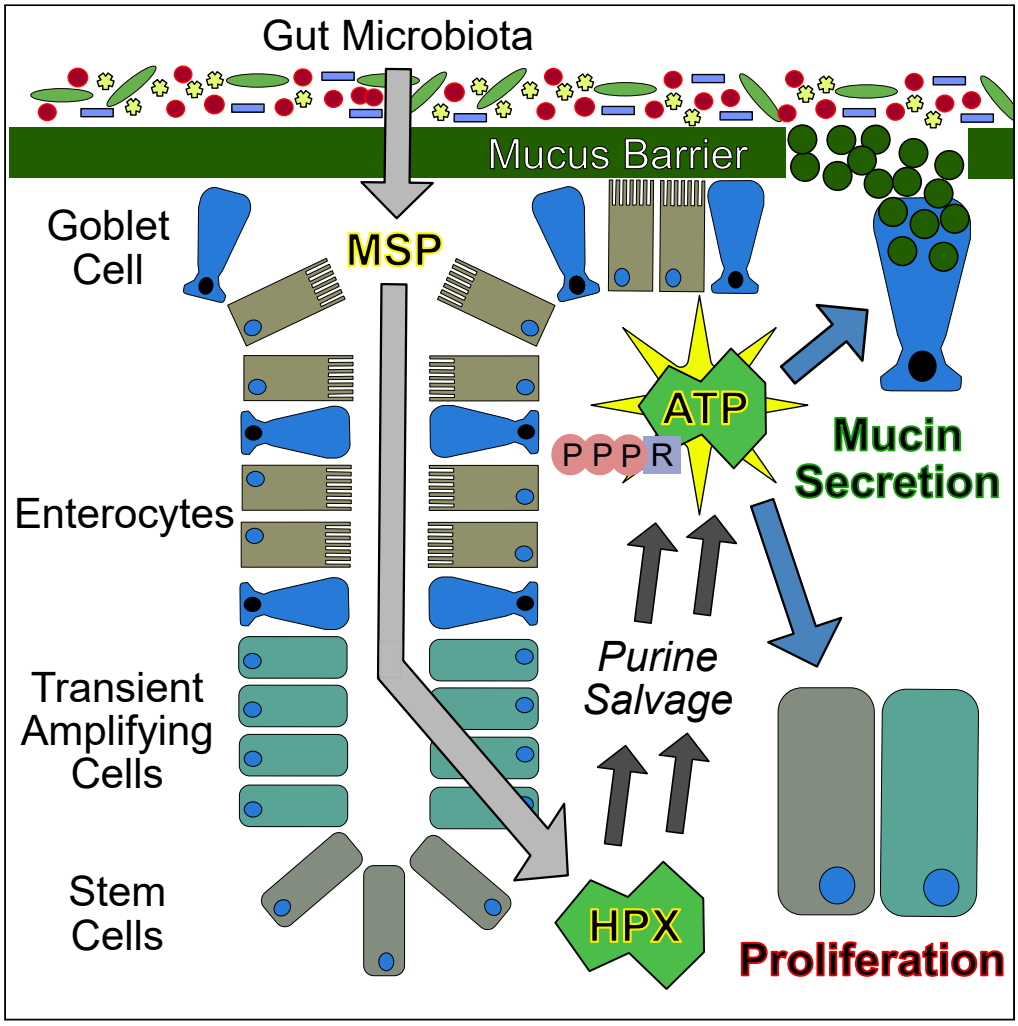

J. Scott Lee, Ruth X. Wang, Matthew S. Goldberg, Garrett P. Clifford, Daniel J. Kao, Sean P. Colgan

sean.colgan@cuanschutz.edu

HIGHLIGHTS

The gut microbiota releases purine compounds available to the host mucosal tissue

Microbiota-sourced purines (MSPs) are salvaged by the gut mucosa for nucleotide genesis

MSPs support energy balance, proliferation, and mucous barrier function

Supplementation with hypoxanthine recapitulates the benefits afforded by MSPs

Lee et al., iScience *23*, 101226
June 26, 2020
https://doi.org/10.1016/j.isci.2020.101226

iScience

CellPress
OPEN ACCESS

Article

Microbiota-Sourced Purines Support Wound Healing and Mucous Barrier Function

J. Scott Lee,[1] Ruth X. Wang,[1] Matthew S. Goldberg,[1] Garrett P. Clifford,[1] Daniel J. Kao,[1] and Sean P. Colgan[1,2,*]

SUMMARY

The intestinal mucosa requires high levels of nucleotides for energy procurement, proliferation, and innate immunity. This need for nucleotide substrates substantially increases during injury, infection, and wound healing. In the present studies, we profile potential sources of purine nucleotides in murine mucosal tissue. This work reveals the gut microbiota as a prominent source of exogenous purines and that such microbiota-sourced purines (MSPs) are available to the intestinal mucosa. The MSPs are utilized for nucleotide genesis and promote energy balance. Further analyses reveal that colitic tissues lacking MSPs are proliferatively stunted, with notable energetic and endoplasmic reticulum stress to the detriment of mucous barrier integrity. Purine reconstitution either directly or through colonization of germ-free/antibiotic-treated mice with MSP-sufficient *E. coli* alleviates such deficits, establishing MSP as a critical source of substrate for tissue metabolism, wound healing, and mucous barrier sterile integrity.

INTRODUCTION

Microorganisms comprising the commensal microbiota of the gut exist in a symbiotic relationship with the host (Kazimieras Malys et al., 2015). This intimate relationship has developed over millions of years of coevolution (Artis, 2008; Hooper and Macpherson, 2010). As such, the intestinal epithelium does not maintain homeostasis in an entirely immanent manner and instead relies upon microbiota-derived molecules to provide nutrients for metabolism and signaling (Maloy and Powrie, 2011). For instance, bacterial fermentation of dietary fiber provides the short-chain fatty acid butyrate, which is not only utilized by the colonic epithelium as an energy substrate through oxidative phosphorylation but also regulates epithelial transcription through histone deacetylase inhibition and activation of G protein-coupled receptors (Kelly et al., 2015; Kim et al., 2013; Macia et al., 2015; Schilderink et al., 2016; Tan et al., 2014).

The large intestine must simultaneously provide habitat for and protect against the gut microbiota to maintain homeostasis and does so by constructing barriers to isolate commensal microbes from the underlying host immune system. Two primary differentiated colonic epithelial cell types shoulder the burden of barrier formation and maintenance—the goblet cell and enterocyte. Goblet cells are responsible for secreting large quantities of mucin, and in doing so simultaneously build the first line of defense against and provide habitat for the microbial species in the gut. This action covers the colonic epithelium with a dense, inner glycocalyx of epithelial-anchored, polymerized MUC2 mucin that establishes a boundary inaccessible to most luminal microbes, which eventually thins to form an outer, less-dense layer that provides habitat and food for commensal bacteria (Johansson et al., 2008; Okumura and Takeda, 2017; Pelaseyed et al., 2014). Enterocytes contribute to barrier by polarizing and forming the apical intercellular tight and adherens junctions that constitute the apical junction complex (AJC) to regulate cell-cell adhesion and paracellular ion transport (Hartsock and Nelson, 2008; Laukoetter et al., 2008; Suzuki, 2013). Insufficient mucin secretion and dysregulation of paracellular flux are foundational tenets of inflammatory bowel disease (IBD) pathophysiology (Groschwitz and Hogan, 2009; Kaser et al., 2010; Meddings, 1997; Schmitz et al., 1999). Although the etiology of IBD remains elusive, restoration of intestinal barrier is paramount for inflammatory resolution and a return to intestinal homeostasis.

Intestinal wound healing and mucin barrier restoration require substantial nucleotide genesis to provide DNA for proliferation and RNA for protein transcription. Furthermore, ATP biosynthesis and regeneration are required at a high level to sustain an energy balance conducive to cytoskeletal function for wound restitution and endoplasmic reticulum (ER) function for mucin formation and

[1]Department of Medicine and the Mucosal Inflammation Program, University of Colorado School of Medicine, Anschutz Medical Campus, 12700 East 19th Avenue, MS B-146, Aurora, CO 80045, USA

[2]Lead Contact

*Correspondence: sean.colgan@cuanschutz.edu

https://doi.org/10.1016/j.isci.2020.101226

secretion, among numerous other anabolic activities. The adenine nucleotides (AMP, ADP, and ATP) are of exceptional significance to eukaryotic cells. These nucleotides are connected to every process in a living cell, in many cases by directly harnessing the stored energy in ATP to drive chemical reactions, and also by sensing their ratios as a measure of energetic state to balance catabolic and anabolic metabolic activities accordingly (Atkinson, 1977). Our recent work revealed that purine supplementation significantly improved intestinal epithelial cell (IEC) wound healing and barrier restitution capabilities (Lee et al., 2018). Cultured IECs exhibited a strong capacity to improve energy balance by salvaging the purine hypoxanthine (Hpx) for ATP biosynthesis, which in turn supported barrier function and wound healing. In extension of that work, we herein identify Hpx as an immediate product of the intestinal microbiota. Through a series of *in vivo* experiments involving microbiota-sourced purine (MSP) depletion, and reconstitution directly (Hpx supplementation) or indirectly (colonization with purine-producing bacteria), we delineate the essential contribution of MSP to colonic epithelial proliferation, energy balance, and mucin barrier integrity.

RESULTS

Intestinal Microbiota Produce and Release Purines at High Levels

Our previous work identified Hpx as a checkpoint metabolite during epithelial barrier restitution (Lee et al., 2018). These studies revealed that after disturbing the epithelial barrier, Hpx rapidly pooled and provided a readily available energy source to drive barrier reformation. In the current studies, we sought to identify potential sources of purines within the murine mucosa. Surprisingly, high-performance liquid chromatography analyses of water-soluble, extracellular fecal metabolites from conventionally raised (CR) mice identified substantial levels of readily salvageable, available purine, primarily as Hpx (~360 nmol/g feces) and xanthine (Xan, ~100 nmol/g feces; CR-CNTL). The production of purines by the microbiota was verified in fecal extracts of streptomycin-treated mice (S-CR-CNTL), which decreased available fecal purine by nearly 90%, lowering Hpx to <50 nmol/g ($p = 0.008$) and Xan to 26 nmol/g ($p < 0.002$). Fecal analyses of germ-free (GF) mice revealed almost undetectable levels of available purine (Hpx and inosine [Ino] <5 nmol/g, $p = 0.004$; Xan not detected, $p < 0.001$; GF-CNTL; Figure 1A). Such results identify, for the first time, the existence of soluble extracellular purines derived from the microbiota.

The Colonic Mucosa Salvages Supplemented Purine for Nucleotide Genesis

Cells sense their relative adenine nucleotide levels as a marker of energetic state and functional capability to tune ATP-consuming and ATP-generating processes accordingly. The adenylate energy charge (AEC, (ATP + 0.5×ADP)/(ATP + ADP + AMP)) is a commonly used index defined by relative adenine nucleotide levels that indicates cellular energy status, providing a functionally relevant metric of energy balance and thus functional capacity (Atkinson and Walton, 1967). To assess the influence of purine supplementation on colonic adenylate and energy metabolism in the absence of the microbiota, GF mice were administered 1 mM Hpx *ad libitum* in the drinking water for 1 week and colon tissues harvested for metabolite analyses. Previous studies revealed that 1 mM Hpx supplementation in CR mice significantly influenced colonic adenylate nucleotide levels, raising the AEC from ~0.52 to 0.72 (Lee et al., 2018). This Hpx supplementation in GF mice similarly impacted colonic nucleotide levels, with AMP decreasing from 74 to 60 nmol/g ($p = 0.04$) and ATP increasing from 83 to 105 nmol/g ($p = 0.05$) to shift the AEC from 0.52 to 0.60 ($p = 0.01$; Figures 1B and 1C). Other adenylate and energy metabolites (Hpx, Xan, Ino, ADP, and phosphocreatine [PCr]) were not significantly altered. AEC increasing as the primary metabolic outcome of oral Hpx supplementation in GF and CR mice suggests that mucosal purine salvage for ATP genesis occurs independent of the gut microbiota. To further observe the metabolism of purine salvage, MSPs were depleted by administering streptomycin to CR mice (S-CR-CNTL; as in Figure 1) followed by reconstitution by administration of Hpx (S-CR-1 mM HPX) by enemas at time points of 5 and 18 h before sacrifice, representing a relatively acute purine treatment in comparison to oral supplementation. The administered Hpx was incorporated into the adenine nucleotide pool of distal colonic tissue, increasing AMP (58–84 nmol/g, $p = 0.02$) and ADP (80–123 nmol/g, $p < 0.02$), whereas ATP was decreased (192–154 nmol/g, $p < 0.02$; Figure 1D). These adenylate metabolite shifts were accompanied by a substantial PCr decrease (3,700–2,000 nmol/g, $p < 0.05$; Figure 1E). The adenylate and energy metabolite shifts incurred by this acute Hpx supplementation offer a snapshot of the enzymatic mechanisms, especially the adenylate and creatine kinases, employed to salvage purine for ATP genesis (Figures 1F and S1). Notably, the disproportionate PCr decrease is indicative of purine supply stimulating energy consumption beyond that needed for salvage-driven ATP biosynthesis.

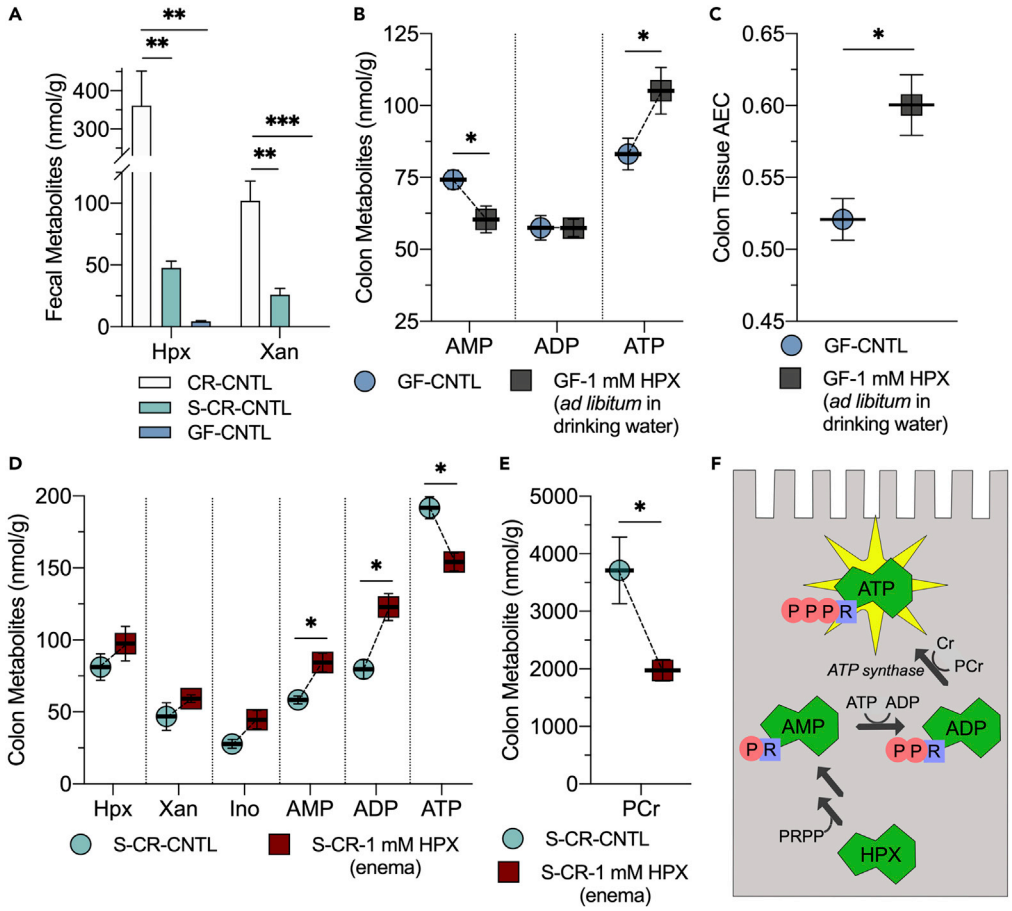

Figure 1. Identification of Microbiota-Sourced Purines (MSPs) and the Impact of Purine Supplementation on Energy Metabolism

(A) Extracellular hypoxanthine and xanthine in murine fecal extracts from conventionally raised (CR), CR streptomycin-treated (S-CR-CNTL), and germ-free (GF) mice (GF-CNTL; n = 5).

(B) Adenylate nucleotide shifts in GF mice orally supplemented with 1 mM Hpx *ad libitum* in drinking water (GF-1 mM HPX; n = 5).

(C) Adenylate energy charge shifts in GF mice orally supplemented with 1 mM Hpx *ad libitum* in drinking water (n = 5).

(D) Colon tissue adenylate metabolite analyses of streptomycin-treated mice (S-CR-CNTL) administered 1 mM hypoxanthine by enema (S-CR-1 mM HPX; n = 3).

(E) Colon tissue phosphocreatine analyses of S-CR-CNTL mice administered 1 mM hypoxanthine by enema (n = 3).

(F) Graphical summarization of hypoxanthine salvage for ATP genesis. Data are represented as mean ± SEM. *p < 0.05, **p < 0.01, ***p < 0.001; Hpx, hypoxanthine; Xan, xanthine, Ino, inosine; AMP, adenosine monophosphate; ADP, adenosine diphosphate; ATP, adenosine triphosphate; PCr, phosphocreatine, Cr, creatine; PRPP, phosphoribosyl pyrophosphate.

Purine-Producing Bacteria Protect against Dextran Sodium Sulfate-Induced Colitis

To assess the contribution of MSP in colonic metabolism and function, GF-CNTL mice were monocolonized with *E. coli* K12 (GF-K12). Apparent available fecal purine was determined, identifying K12 production of Xan (undetected to 14 nmol/g, $p < 0.001$) and Ino (3.6–28 nmol/g, $p < 0.001$), raising the total apparent available fecal purine from 8.0 to 46 nmol/g ($p < 0.001$; Figure 2A). The GF-CNTL and GF-K12 mice were then subjected to dextran sodium sulfate (DSS) colitis, throughout which the colonized mice showed minimal clinical symptoms of colitis, whereas the uncolonized mice succumbed to disease (Figures 2B and 2C).

Despite K12 providing roughly a tenth of the available purine provided by commensals in CR mice, GF-K12 mice showed significant increases in colon tissue Hpx (48–160 nmol/g, $p < 0.005$), Xan (22–66 nmol/g, $p <$

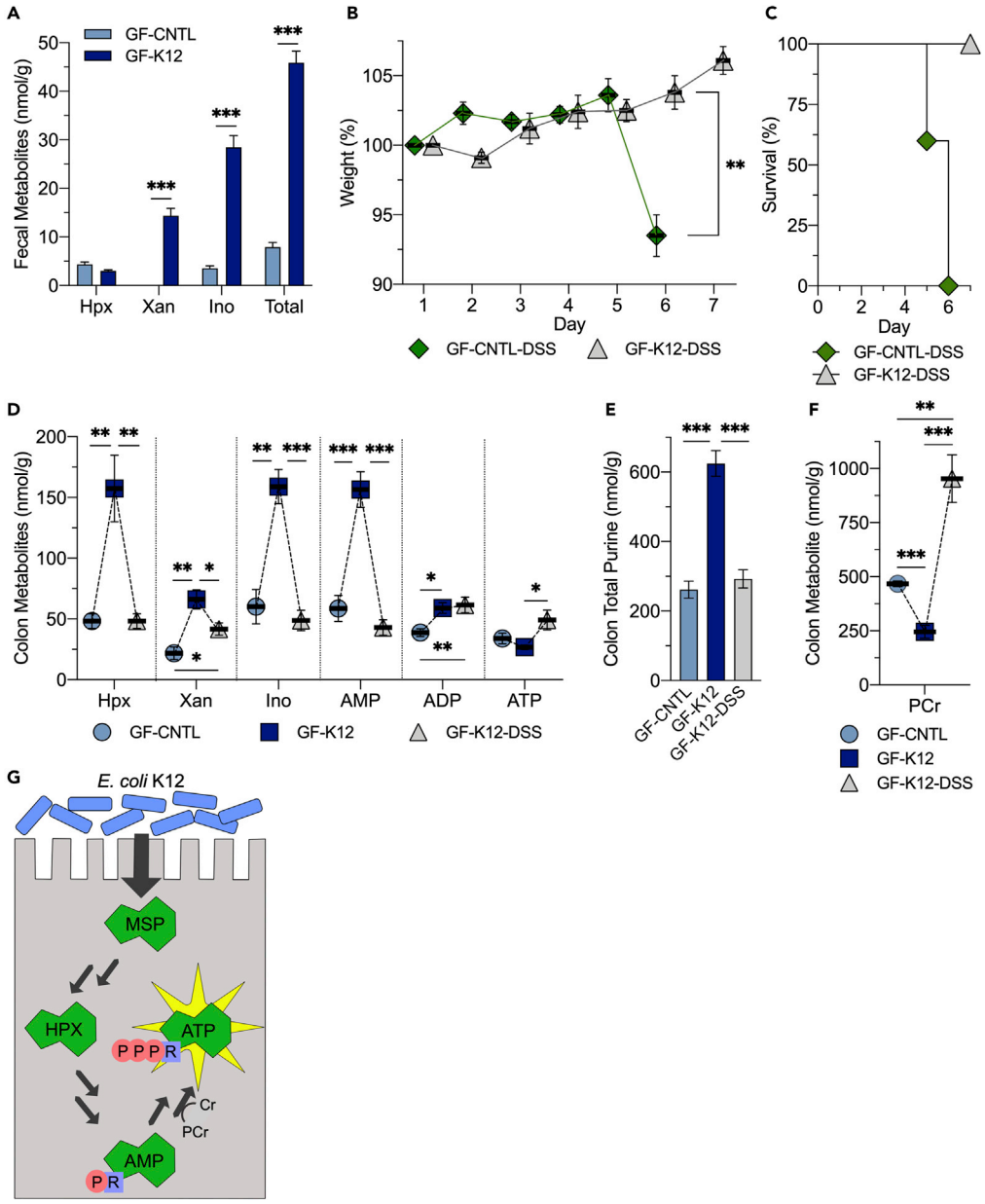

Figure 2. MSPs Protect against DSS Colitis in Germ-Free Mice

(A) Extracellular fecal purine metabolite analyses of GF-CNTL and GF mice colonized with *E. coli* K12 (GF-K12).

(B) Weight curves of GF-CNTL and GF-K12 mice subjected to DSS colitis (GF-CNTL/K12-DSS; n = 5).

(C) Survival curves of GF-CNTL-DSS and GF-K12-DSS mice subjected to DSS colitis.

(D) Colon tissue adenylate metabolite analyses of GF-CNTL, GF-K12, and GF-K12-DSS mice.

(E) Total purine metabolite levels from GF-CNTL, GF-K12, and GF-K12-DSS extracts. Total purine is the sum of adenylate metabolites presented.

(F) Colon tissue phosphocreatine analyses of GF-CNTL, GF-K12, and GF-K12-DSS mice.

(G) Graphical summary of MSP salvage for ATP genesis. Data are represented as mean ± SEM (n = 5). *p < 0.05, **p < 0.01, ***p < 0.001; Hpx, hypoxanthine; Xan, xanthine, Ino, inosine; AMP, adenosine monophosphate; ADP, adenosine diphosphate; ATP, adenosine triphosphate; PCr, phosphocreatine; Cr, creatine.

0.002), Ino (60–159 nmol/g, p = 0.001), AMP (59–157 nmol/g, p < 0.001), and ADP (39–59 nmol/g, p < 0.006), raising the total purine from 260 to 620 nmol/g (p < 0.001), which elevated the formerly purine-deficient tissue to a level comparable to that observed in CR mice (~800 nmol/g). In addition, GF-K12 mice showed

a corresponding colonization-induced PCr decrease from 470 to 250 nmol/g ($p < 0.001$; Figures 2D–2F). Fecal extract analyses showed that K12 monocolonization supplied purines to the colon in the form of Ino and Xan instead of the Hpx and Xan observed in CR mice, but the Hpx increase observed in the GF-K12 colon tissue signifies that the available Ino incorporated into the adenine nucleotide pool through Hpx as an intermediate, and therefore through the purine salvage pathway (Figures 2G and S1). Accordingly, analyses of T84 IECs treated with 100 μM ADP or 1 mM adenosine resulted in ~15- and over 150-fold Hpx increases, respectively (unpublished). The colonization of GF mice with purine-producing bacteria induced metabolite shifts similar to those observed in the GF oral Hpx supplementation and CR Hpx enema model, with K12-derived purine supply appearing to strike a balance between the two. The targeted delivery of purines via bacterial colonization or enema in purine-depleted mice increased colonic purine nucleobase, nucleoside, and AMP levels, but the influx of K12-supplied purine was not substantial enough to incur ATP depletion. On the whole, the luminally supplied purine was incorporated into the colonic tissue, and as manifested by increased PCr consumption, appeared to fuel and promote energy use.

Colon tissue metabolite analyses of colonized mice subjected to DSS colitis (GF-K12-DSS) showed reduced total purine levels (620–290 nmol/g, $p < 0.001$) but maintenance of ADP, with elevated ATP (27–50 nmol/g, $p < 0.05$) and PCr (250–953 nmol/g, $p < 0.001$), suggesting that the tissue utilized the MSP to exhaustion in an effort to maintain di- and triphosphate adenylate nucleotide levels, and thus energetic capacity, during insult (Figures 2D–2F).

Maintenance of Energy Balance Is Key to the Protection Conferred by MSP against DSS Colitis

Given the protection against DSS colitis afforded by colonization of GF mice with the purine producing *E. coli*, we extended our analyses to a CR mouse model. Bacterial supply of purine was depleted in CR mice (CR-CNTL) via streptomycin treatment (S-CR-CNTL) and reconstituted by colonization with streptomycin-resistant K12 (S-CR-K12). In agreement with the GF model, the K12-colonized CR mice were protected from DSS, showing minimal clinical symptoms of colitis (Figure 3A). Colon lengths are commonly decreased during DSS colitis and may be used as a metric of disease severity. The S-CR-K12 mice showed the least amount of colon shortening (~4%), with streptomycin alone blunting the decrease (~8%) compared with CR-CNTL (~13%; $p < 0.05$ between all groups; Figure 3B). At baseline, total colonic purine levels decreased from 809 to 630 nmol/g ($p = 0.01$) upon streptomycin-induced MSP depletion, primarily in the form of Xan (207–69 nmol/g, $p < 0.001$). Purine levels were recovered to 750 nmol/g ($p = 0.05$) with K12 colonization (Xan: 148 nmol/g, $p = 0.003$).

Upon subjection to DSS colitis, the K12-colonized mice significantly drew from the total purine store (750–570 nmol/g, $p < 0.008$), while the CR-CNTL mice trended similarly (809–694 nmol/g; Figure 3C). The CR-CNTL mice appeared to utilize the purine reserve to maintain ATP throughout the insult, as revealed through reductions in colon tissue Xan (207–111 nmol/g, $p < 0.002$), AMP (145–60 nmol/g, $p < 0.001$), and ADP (113–83 nmol/g, $p < 0.008$). The S-CR-K12 mice exhibited a similar maintenance of ATP as seen in the CR-CNTL group but with an additional decrease in Hpx (239–158 nmol/g, $p < 0.04$) along with Xan (148–86 nmol/g, $p < 0.001$), AMP (128–43 nmol/g, $p < 0.001$), and ADP (104–78 nmol/g, $p < 0.004$). In contrast, the S-CR-CNTL mice distinctively lacked purine salvage for ATP genesis, appearing unable to draw from cellular Hpx, Xan, and ADP, and employed AMP to a lesser extent (128–88 nmol/g, $p < 0.004$), rendering the tissue unable to maintain ATP throughout the insult (90–61 nmol/g, $p < 0.01$). Interestingly, all experimental groups showed a 2.5- to 4-fold Ino increase ($p < 0.01$ across all groups) in response to the insult, analogous to *in vitro* work wherein IECs subjected to stress (hypoxia and 2-deoxyglucose) showed substantial Ino increases (Lee et al., 2018). DSS colitis significantly depleted colon tissue energy stores, decreasing PCr ~400 nmol/g ($p < 0.01$) in all mouse groups. In accordance with the GF model, MSP supply itself decreased PCr (~150 nmol/g) at baseline and after insult, further indicative of exogenous purine salvage driving metabolite flux through ATP, with this flux necessary to maintain ATP during insult and recovery (Figure 3D). Furthermore, the AEC correlated with MSP supply during insult accordingly. CR-CNTL mice subjected to DSS (CR-CNTL-DSS) showed an AEC of 0.51, which decreased to 0.44 ($p < 0.04$) with MSP depletion (S-CR-CNTL-DSS), and then recovered to 0.57 ($p < 0.001$) with purine reconstitution by K12 colonization (S-CR-K12-DSS; Figure 3E). These results further demonstrated that MSPs support ATP biosynthesis and an energy balance conducive to an anabolic, wound-healing state during insult and recovery.

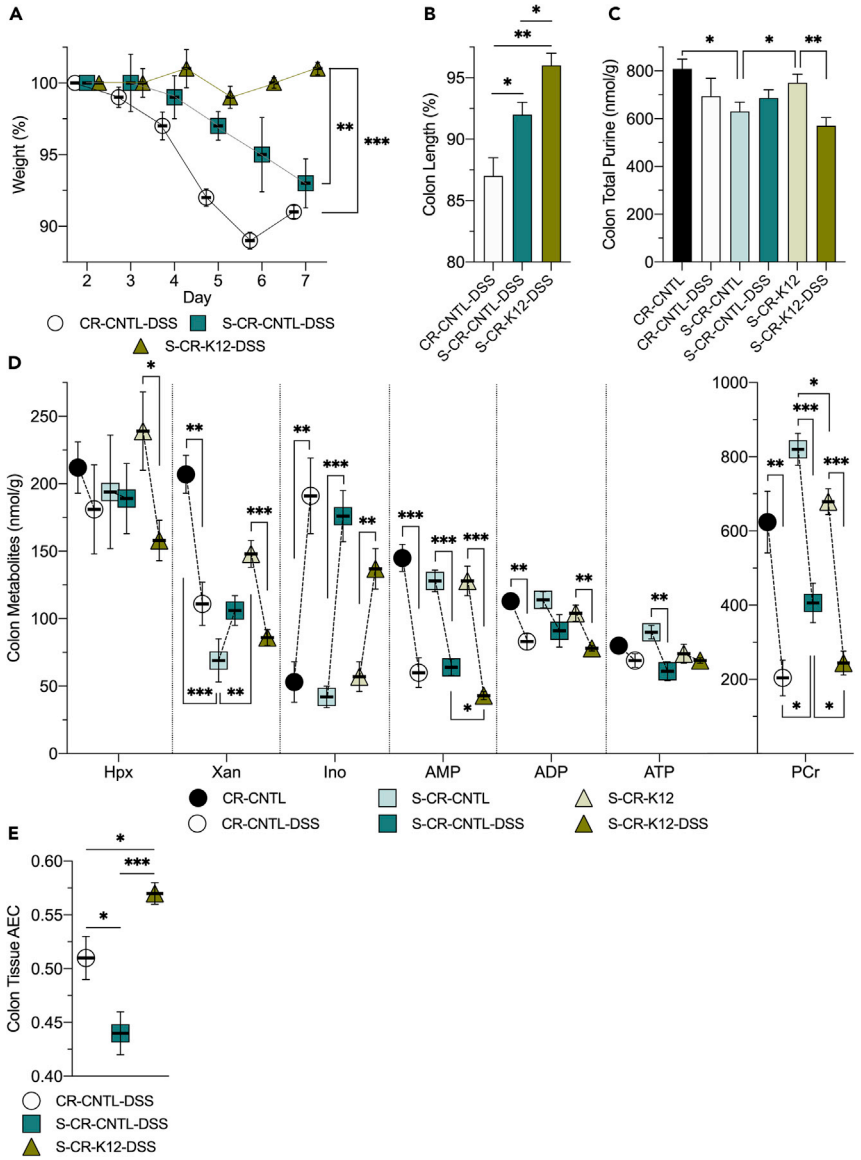

Figure 3. MSPs Protect Conventionally Raised Mice against DSS Colitis and Promote Energy Balance

(A) Weight curves of conventionally raised control (CR-CNTL-DSS), streptomycin-treated control (S-CR-CNTL-DSS), and streptomycin-treated, K12-colonized (S-CR-K12-DSS) mice subjected to DSS.

(B) Colon length shortening incurred by DSS colitis in the CR mouse cohort.

(C) Total purine metabolite levels extracted from colon tissues of non-DSS and DSS-administered mice. Total purine is the sum of adenylate metabolites presented.

(D) Adenylate and energy metabolite levels extracted from colon tissues of non-DSS and DSS-administered mice.

(E) Adenylate energy charge determined from the murine colon tissues subjected to DSS. Data are represented as mean ± SEM (n = 5). *p < 0.05, **p < 0.01, ***p < 0.001; Hpx, hypoxanthine; Xan, xanthine, Ino, inosine; AMP, adenosine monophosphate; ADP, adenosine diphosphate; ATP, adenosine triphosphate; PCr, phosphocreatine; AEC, adenylate energy charge.

MSPs Support Proliferation and Mitigate Apoptosis to Drive Mucosal Healing

Histological scores among the CR mouse groups did not reveal significant differences in colonic disease activity, but visualization of the colon tissues by hematoxylin and eosin (H&E) staining in the CR mouse groups revealed two key differences between tissues with and without MSPs. First, the streptomycin control mice treated with DSS showed shorter crypt depths with fewer epithelial cells, ensuing in a thinner,

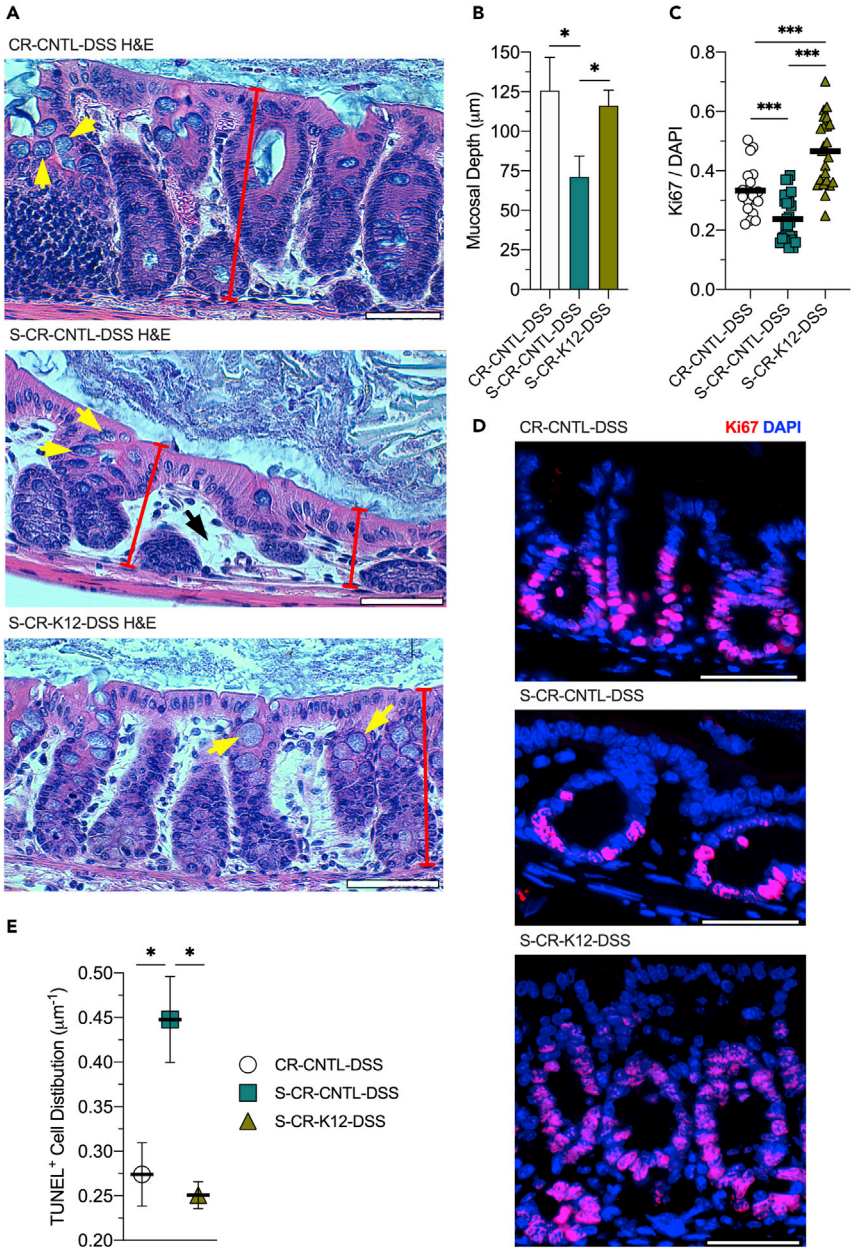

Figure 4. Proliferation Is Supported and Apoptosis Attenuated by MSPs

(A) Representative hematoxylin and eosin (H&E) staining images of conventionally raised control (CR-CNTL-DSS), streptomycin-treated control (S-CR-CNTL-DSS), and streptomycin-treated, K12-colonized (S-CR-K12-DSS) mice subjected to DSS. Yellow arrows indicate goblet cell theca, red bars represent crypt depth, and black arrows highlight the lack of epithelial cell density.

(B) Mucosal depth measurements of the CR-DSS mouse cohort. Data are represented as mean ± SEM (n = 45).

(C) Immunofluorescence analyses of the CR-DSS mouse cohort targeting Ki67. Data are represented as mean (n = 19–29).

(D) Representative images of the CR-DSS mouse cohort Ki67 immunofluorescent analyses. Scale bars, 50 μm.

(E) Distribution of TUNEL-positive mucosal cells across the mouse groups. Data are represented as mean ± SEM (n = 4).

*p < 0.05, **p < 0.01, ***p < 0.001.

less-dense mucosa. Second, goblet cell thecal volume was noticeably attenuated, suggesting dysfunctional mucin production (Figure 4A). Concomitant with the H&E observations, mucosal depth measurements across the CR-DSS mouse cohort revealed a substantial decrease upon streptomycin treatment (126–71 μm, $p < 0.04$) that was recovered by K12 colonization (116 μm, $p = 0.03$; Figure 4B).

Insult to the intestinal epithelium not only depletes energy, requiring substantial ATP regeneration, but also demands considerable nucleotide genesis for cellular proliferation to repopulate and heal the mucosa. As the AEC was significantly changed in the aforementioned models and adenylate energetics is instrumental in balancing catabolism and anabolism, impacting cell growth, the colon tissue analyses were extended to Ki67 as a marker of proliferation. Immunofluorescence analyses of the DSS-insulted tissues revealed a substantial decrease in proliferation upon MSP depletion (0.33–0.24 Ki67/DAPI, $p < 0.001$). The proliferative capacity was recovered by K12 colonization and reconstitution of MSP supply (0.47 Ki67/DAPI, $p < 0.001$; Figures 4C and 4D). To assess the contribution of MSP to apoptosis, TUNEL staining was performed on tissue sections and the number of TUNEL-positive cells on each cross section was normalized to mucosal depth. Depletion of purine supply increased the distribution of apoptotic cells (0.27–0.44 μm^{-1}, $p = 0.04$), which was reversed by K12 colonization (0.25 μm^{-1}, $p < 0.02$; Figure 4E). Taken together, colon tissues lacking MSPs were appreciably unable to repopulate the epithelial cell population and were less resistant to apoptosis.

Decreased ER Stress Promotes Goblet Cell Function and Mucous Barrier Sterility

The ER is notably reliant on ATP to execute protein-related functions. Without sufficient ATP, misfolded proteins accumulate, dock to binding immunoglobulin protein (BiP), and induce a signal transduction pathway called the *unfolded protein response* (UPR) (Hetz and Papa, 2018). The ATP-dependent BiP blocks ER stress signaling, assists protein folding, protects against misfolded protein toxicity, and is also upregulated by the UPR (Rao and Bredesen, 2004). As ATP supply is intricately linked to ER function, colon tissues from the CR-DSS mouse cohort were analyzed for BiP immunofluorescence as a marker of ER stress and the UPR. BiP protein was indeed elevated by MSP depletion, rising from 0.33 to 0.44 BiP/DAPI ($p < 0.001$), which was attenuated by K12 MSP reconstitution, lowering BiP levels to 0.34 BiP/DAPI ($p = 0.01$; Figures 5A and 5B).

Given the reduction in goblet cell thecal volumes seen in the H&E sections and need for robust ER function for mucin protein folding and dimerization (Javitt et al., 2019), the impact of MSP on colonic mucin production and secretion was assessed through Alcian blue staining of mucin in tissue sections. The staining also revealed a broad decline in goblet cell thecal volumes as a consequence of MSP depletion, which was recovered by K12 reconstitution of MSP supply (Figure 5C). Immunofluorescent staining of *E. coli* was used to indicate sterile integrity of the inner mucin layer and estimate the penetration of the mucous barrier by members of the gut microbiota. The average depth of the sterile mucous layer in the CR-CNTL-DSS mice was ~7 μm, which decreased to ~2 μm ($p = 0.008$) upon MSP depletion. K12 colonization rescued mucous barrier sterility, increasing the depth to ~5 μm ($p < 0.03$; Figures 5D and 5E). Across the images analyzed, an additional metric termed sterility index was assessed in that if no *E. coli* contacted with the epithelium, a score of 1 was given, whereas if contact existed at any point in an image, a score of 0 was given. MSP supply correlated with the sterility index, with CR-CNTL-DSS and S-CR-K12-DSS mice scoring ~0.5, as opposed to the MSP-depleted mice scoring ~0.1 ($p < 0.02$ and $p = 0.04$, respectively; Figure 5F). In this, MSPs demonstrated an essential role in the mucin formation and secretory capability of colonic goblet cells with significant implication on the sterile integrity of the mucous barrier.

Hypoxanthine Supplementation in MSP-Depleted Mice Independently Recapitulates the Benefits of K12 Colonization

To validate the role of exogenous purine supply independent of the colonization process on colonic function, streptomycin-treated mice (S-0 mM HPX-DSS) were supplemented with 1 mM Hpx (S-1 mM HPX-DSS) in their drinking water and subjected to DSS colitis. Mice receiving no Hpx supplementation lost ~9% of their body weight throughout the course of the experiment, whereas supplementation with 1 mM Hpx was protective, with mice losing ~3% of their body weight ($p < 0.02$; Figure 6A). The S-0 mM HPX-DSS group had colon lengths of ~5.8 cm, whereas supplementation appeared protective, with 1 mM Hpx-supplemented mice exhibiting a length of ~6.3 cm ($p = 0.03$; Figure 6B).

Similar to K12 colonization, 1 mM Hpx increased the AEC from 0.30 to 0.38 ($p = 0.02$; Figure 6C). H&E staining of colonic tissue revealed similar phenotypes as the K12-colonized mice, with Hpx supplementation also recovering the loss of epithelial cell population and lack of mucin production incurred with streptomycin (Figures 6D and 6E). As anticipated, 1 mM Hpx increased tissue proliferation from 0.22 to 0.54 Ki67/DAPI in response to DSS ($p < 0.001$; Figures 6F and 6G), and the direct purine supply halved the distribution of TUNEL-positive cells (0.47–0.22 μm^{-1}, $p < 0.02$; Figure 6H). Salvage of the exogenous Hpx and the resulting AEC shifts also impacted ER stress, with 1 mM Hpx supplementation decreasing BiP from 0.41 to 0.23 ($p < 0.001$; Figures 7A and 7B). The positive influences on tissue AEC and ER stress afforded by Hpx

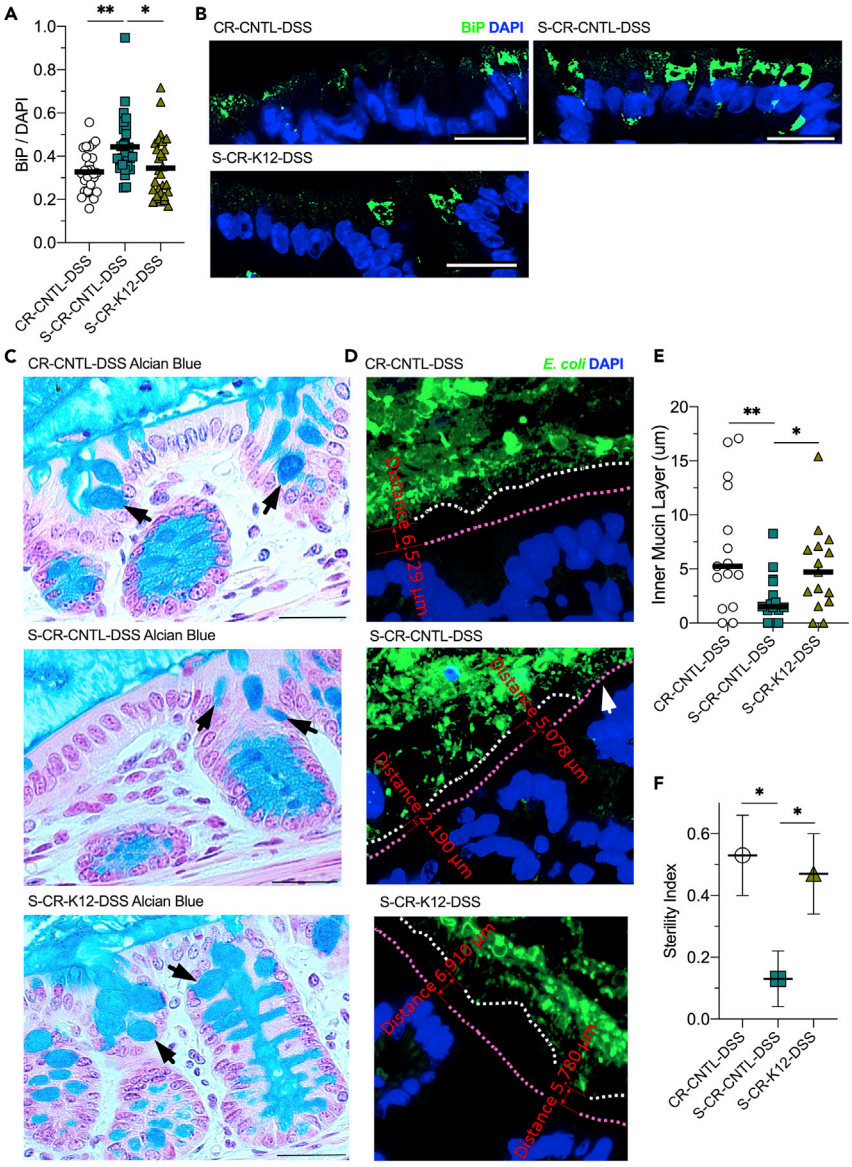

Figure 5. MSPs Alleviate ER Stress and Promote Mucous Barrier Sterility

(A) Immunofluorescent analyses of conventionally raised control (CR-CNTL-DSS), streptomycin-treated control (S-CR-CNTL-DSS), and streptomycin-treated, K12-colonized (S-CR-K12-DSS) mice subjected to DSS targeting binding immunoglobulin protein (BiP). Data are represented as mean (n = 28).

(B) Representative images of the CR-DSS mouse cohort BiP immunofluorescent analyses. Scale bars, 50 μm.

(C) Representative images of mucin staining of tissues from the CR-DSS mouse cohort by Alcian blue and nuclear fast red. Black arrows indicate goblet cell theca. Scale bars, 100 μm.

(D) Representative immunofluorescence images targeting *E. coli* and associating inner mucin layer depth measurements of the CR-DSS mouse cohort. Magenta line highlights the mucosal surface, white line highlights the end of the inner mucin layer, and white arrow indicates a region of contact between the microbiota and epithelium.

(E) Inner mucin layer depth measurements of the CR-DSS mouse cohort. Data are represented as mean (n = average of 5 measurements across 15 images).

(F) Sterility index of the CR-DSS mouse cohort mucous barrier. Data are represented as mean ± SEM (n = 15). *$p < 0.05$, **$p < 0.01$.

supplementation correlated with increased goblet cell mucin production and secretion, as observed by increased thecal volumes (Figure 7C) and increased sterile region thickness, with 1 mM Hpx supplementation increasing the sterile inner mucin layer from ~1 to 9 μm ($p < 0.001$; Figures 7D and 7E). Accordingly, the

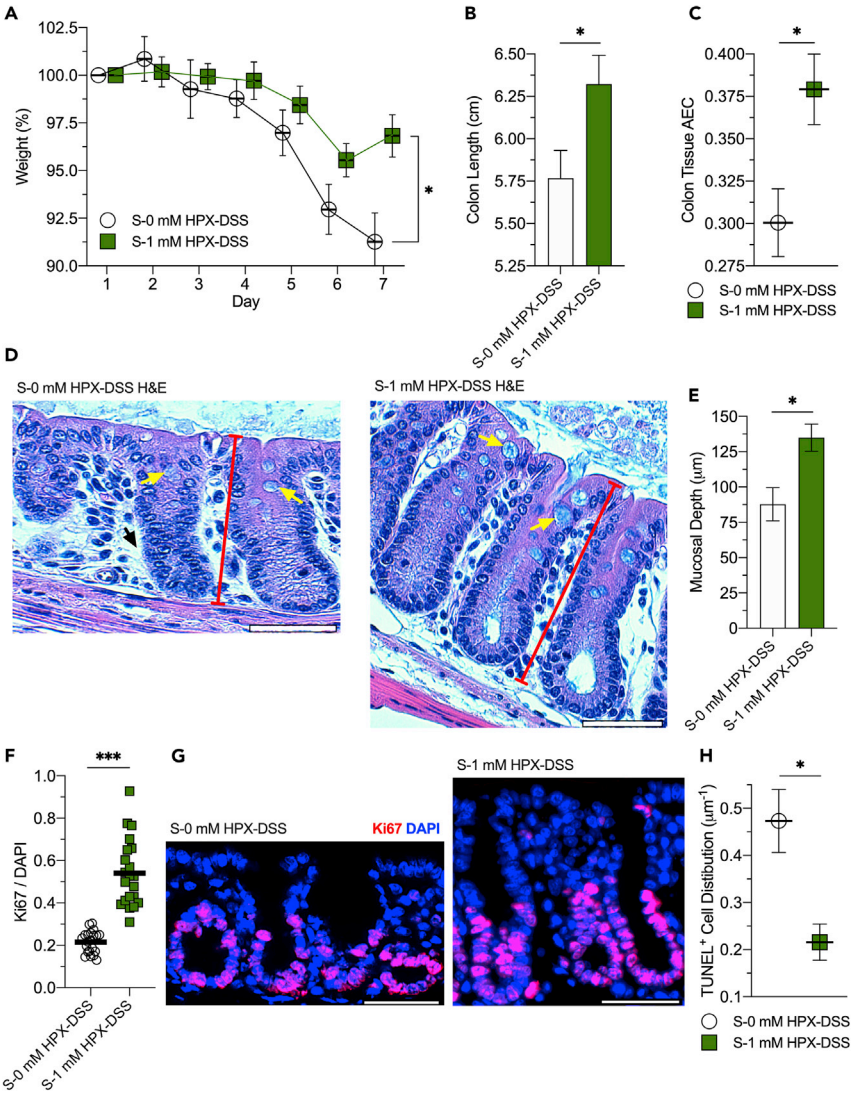

Figure 6. Hypoxanthine Protects MSP-Depleted Mice Against DSS Colitis by Supporting Energy Balance and Proliferation

(A) Weight curves of streptomycin-treated, conventionally raised control (S-0 mM HPX-DSS) and 1 mM hypoxanthine-supplemented (S-1 mM HPX-DSS) mice subjected to DSS. Data are represented as mean ± SEM (n = 5).

(B) Colon lengths of the hypoxanthine-supplemented, DSS-treated mouse cohort. Data are represented as mean ± SEM (n = 5).

(C) Colon tissue adenylate energy charges of the hypoxanthine-supplemented, DSS-treated mouse cohort. Data are represented as mean ± SEM (n = 5).

(D) Representative hematoxylin and eosin (H&E) staining images of the hypoxanthine-supplemented mouse cohort. Yellow arrows indicate goblet cell theca, red bars represent crypt depth, and the black arrow highlights the lack of epithelial cell density.

(E) Mucosal depth measurements of the hypoxanthine DSS mouse cohort. Data are represented as mean ± SEM (n = 44).

(F) Immunofluorescent analyses of S-0 mM HPX-DSS and S-1 mM HPX-DSS mice targeting Ki67. Data are represented as mean (n = 21).

(G) Representative Ki67 immunofluorescent images of the hypoxanthine-supplemented, DSS-treated mouse cohort.

(H) Distribution of mucosal TUNEL-positive mucosal cells across the hypoxanthine DSS mouse groups. Data are represented as mean ± SEM (n = 4).

*p < 0.05, ***p < 0.001. Scale bars, 50 μm.

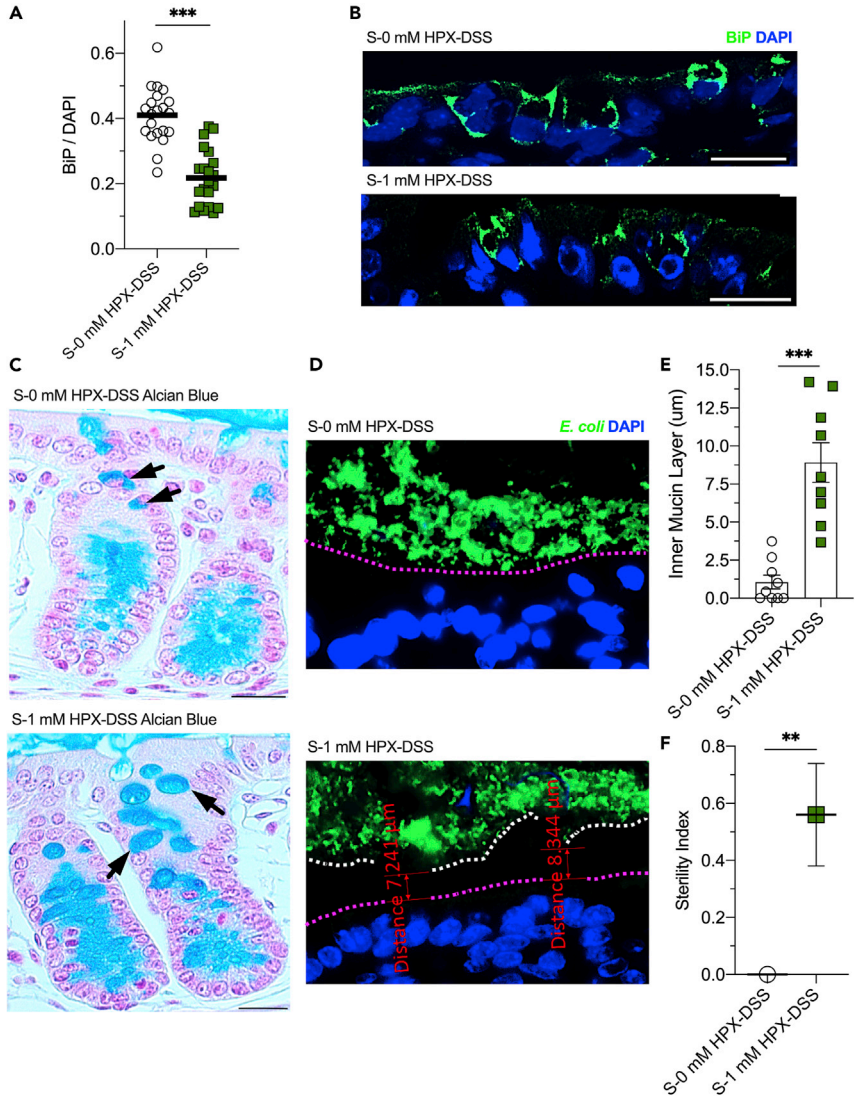

Figure 7. Hypoxanthine Reduces ER Stress and Promotes Mucous Barrier Sterility in MSP-Depleted Mice

(A) Immunofluorescence analyses of streptomycin-treated, conventionally raised control (S-0 mM HPX-DSS) and 1 mM hypoxanthine-supplemented (S-1 mM HPX-DSS) mice subjected to DSS targeting binding immunoglobulin protein (BiP). Data are represented as mean (n = 21).

(B) Representative BiP immunofluorescent images of the hypoxanthine-supplemented, DSS-treated mouse cohort. Scale bars, 50 μm.

(C) Representative images of mucin staining by Alcian blue in S-0 mM HPX-DSS and S-1 mM HPX-DSS mice. Black arrows indicate goblet cell theca. Scale bars, 100 μm.

(D) Representative immunofluorescence images of the hypoxanthine-supplemented, DSS-treated mouse cohort targeting *E. coli*. Magenta line highlights the mucosal surface, white line highlights the end of the inner mucin layer, and white arrow indicates a region of contact between the microbiota and epithelium.

(E) Inner mucin layer depth measurements of the hypoxanthine-supplemented, DSS-treated mouse cohort. Data are represented as mean ± SEM (n = average of 5 measurements across 9 images).

(F) Sterility index of the hypoxanthine-supplemented, DSS-treated mouse cohort. Data are represented as mean ± SEM (n = 9). **$p < 0.01$, ***$p < 0.001$.

1 mM Hpx supplementation promoted mucin barrier integrity, increasing the sterility index from 0 to 0.56 ($p < 0.007$; Figure 7F). Thus, purine supply, regardless of whether through direct (i.e., Hpx supplementation) or indirect (i.e., K12 colonization) routes, protected against DSS-induced weight loss and colon shortening, while also promoting deeper crypts, mucosal cell density, energy balance, ER function, and mucin

secretion, altogether highlighting the distinctive and independent impact of exogenous purine supply on colonic mucosal wound healing and homeostatic function.

DISCUSSION

Metabolites across multiple classes are involved in a complex, chemically mediated crosstalk between the gut microbiota and host tissues, as exemplified by the bile acids, choline, and short-chain fatty acids that are indispensable for health (Nicholson et al., 2012; Nicholson and Wilson, 2003). Significant recent interest in defining active microbial metabolites has driven new technologies and stimulated questions around the complexity of the host microbiome (Ursell et al., 2014). Given the sheer density of microbes in the intestines, colonic epithelial cells are positioned as the primary interface between the host and the environment (Taylor and Colgan, 2017), providing rich opportunities to identify new substrates, modified metabolites, and new mechanisms of host-microbe communication. For instance, identification of Hpx as an energetic checkpoint metabolite in IECs revealed the potential of purine to drive ATP genesis (Lee et al., 2018). Formation and maintenance of the AJC to provide epithelial cell barrier is dominantly reliant on cytoskeletal function and cell energetics (Hartsock and Nelson, 2008; Hirokawa et al., 1983; Ivanov et al., 2010; Juelicher et al., 2007). Given that the *in vitro* Hpx-salvage-driven shift in energetic balance supported IEC cytoskeletal function, imparting increased AJC barrier formation and maintenance as well as wound restitution capabilities, it is reasonable that such a purine-derived energetic benefit could support AJC barrier function *in vivo* and confer protection during DSS. This potential is demonstrated by the present studies, in which we report that MSPs serve an unprecedented role in the mucosa as a conduit for host energy and nucleotide procurement.

Cells that rapidly turnover (i.e., IECs) and secrete large amounts of protein (i.e., mucins) are especially nucleotide demanding, as proliferation requires substantial nucleotide templates to duplicate the genome (DNA), while the production and secretion of large amounts of protein necessitates ample templates for ribosomal RNA generation and transcription (mRNA) (Zhu and Thompson, 2019). Most cells can produce purine nucleotides via two different pathways—the salvage pathway, which utilizes exogenous purine, and the ATP-consuming *de novo* pathway that sequentially constructs purine nucleotides from phosphoribosyl pyrophosphate (PRPP). Previous studies have demonstrated that the gut mucosa preferentially salvages purines *in lieu* of the energy-consuming *de novo* pathway for purine nucleotide genesis given available purine substrate (Grimble, 1994; Lane and Fan, 2015; Mackinnon and Deller, 1973; Savaiano and Clifford, 1981). This preference was recently exemplified by the rapid salvage of supplemented Hpx for ATP genesis by IECs (Lee et al., 2018). Purine salvage begins with the PRPP-dependent ribosylation of Hpx by the action of Hpx-guanine phosphoribosyltransferase (HGPRT) to form inosine monophosphate (IMP), which is either used by the guanylate metabolite pathway for guanosine triphosphate (GTP) biosynthesis or aminated to eventually form ATP. The requirement of GTP for conversion of IMP to AMP functions as a metabolic check on guanylate metabolite levels, shunting purine flux toward GTP biosynthesis if necessary. In this, adenine nucleotide levels function as a marker for all purine nucleotides, as exemplified by the sensing of adenine nucleotide levels as a marker of total levels by mechanistic target of rapamycin complex 1 (mTORC1) in the regulation of mRNA translation (Hoxhaj et al., 2017). Xan is analogously salvaged for GTP production but may also be used to form ATP. *De novo* purine nucleotide biosynthesis initiates with the conversion of PRPP to 5-phosphoribosylamine by amidophosphoribosyltransferase (ATase), utilizing glutamine as an amine donor (Pareek et al., 2020). The purine ring is then sequentially built using small molecule donors, a process that consumes five ATP molecules to eventually form IMP (Figure S1). The preference for nucleotide genesis via the salvage pathway is likely the result of HGPRT having a higher specific activity than ATase, increased affinity for PRPP than ATase, and the allosteric inhibition of ATase by purine nucleotides produced by salvage (Natsumeda et al., 1984; Smith, 1998; Weber et al., 1983, 1987; Yamaoka et al., 1997). Indeed, purine salvage suppresses the *de novo* pathway (Yamaoka et al., 1997). Nonetheless, the colonic mucosa employs the *de novo* pathway to some degree (LeLeiko et al., 1983), and the pathway is likely upregulated in MSP-depleted mice to compensate for the contribution of MSPs to nucleotide genesis. In addition, the *de novo* pathway is expected to be upregulated in response to the decrease in purine nucleotides and increased energetic and proliferative needs incurred by insult (Iwahana et al., 1995), but, as demonstrated by the present studies, the *de novo* pathway cannot fully compensate for the contribution of salvaged MSPs.

In this work, exogenously supplied purines incorporate into murine colonic tissue, generally increasing the corresponding nucleobase, nucleoside, AMP, and ADP levels at baseline. We presume that the decrease in ATP and PCr resulting from the acute Hpx supplementation by enema is indicative of the mechanisms employed to immediately salvage the purines for nucleotide genesis. Adenylate kinase utilizes ATP to convert

the biosynthesized AMP to produce ADP, and then creatine kinase uses PCr to regenerate the consumed ATP and finalize the salvage of Hpx to ATP (Figure S1). In contrast, K12 colonization of GF mice did not significantly influence ATP levels, but substantially decreased PCr, suggestive of purine supply promoting an anabolic metabolism of ATP utilization. This association of PCr consumption with purine salvage-driven nucleotide genesis mirrors *in vitro* IEC work in which inhibition of the salvage pathway increased cellular PCr (Lee et al., 2018). Taken together, the role of creatine kinase in ATP biosynthesis and maintenance confers PCr as a primary gatekeeper and biomarker of flux through ATP.

The protection afforded by the colonization of GF mice with K12 in DSS colitis is striking, with colonized mice showing only minor clinical signs of illness. Adenylate and energy metabolite analyses show that the colon tissue drew from the assimilated MSPs to maintain ATP levels during active inflammation. Extensions of this DSS model into streptomycin-treated and K12-colonized CR mice exhibit a similar response, with the CR colon tissues relying on MSP supply to maintain ATP and energy balance. Although streptomycin does not significantly improve overall weight loss, the treatment appears to alter disease pathogenesis while slightly protecting against colon shortening. Two bacterial phyla comprise over 90% of the human and murine colonic microbiota—*Firmicutes* and *Cytophaga-Flavobacterium-Bacteroidetes* (CFB) (Eckburg et al., 2005; Ley et al., 2005). Administration of streptomycin in the drinking water of mice is reported to not significantly impact the total amount of bacteria in the microbiota, but does work to expand the ratio of CFB in a dose-dependent manner (Sekirov et al., 2008). As inner mucin layer permeabilization and resulting infiltration of bacteria is a fundamental tenant of disease pathogenesis in the DSS colitis model (Johansson et al., 2010), the streptomycin-induced alteration of microbiota composition likely accounts for the protective outcome by reducing or impairing potentially opportunistic commensal bacteria that could contribute to the inflammatory process. Nonetheless, direct and indirect reconstitution of purine supply further improves disease outcome, to the degree that colonization of the streptomycin-treated mice with purine-producing bacteria completely protects against weight loss and further attenuates colon shortening.

The distinct environment of physiological hypoxia in which the colonic mucosa resides is energetically challenging at baseline (Kelly et al., 2015). Generating ATP and maintaining an energy balance conducive to wound healing in a damaging inflammatory setting that entails further hypoxic exacerbation is even more problematic, presenting a substantial obstacle to the essential but nutrient- and energy-consuming processes necessary to regenerate the epithelium and restore lost barrier function. Insufficient ATP production and regeneration manifests as increased ADP and AMP. As such, cellular ATP:ADP and ATP:AMP ratios are sensed as an indicator of energy balance (i.e., functional capability) by the highly conserved master regulator AMP-activated kinase (AMPK) to tune metabolism between an anabolic or ATP-consuming state and a catabolic or ATP-generating state (Garcia and Shaw, 2017; Hardie, 2014; Hardie et al., 2012). In this regard, the AEC serves as a useful index to parse how much ATP is available to support the anabolism necessary to proliferate and repopulate the mucosa and restore or maintain barrier. Salvage of exogenously supplied purines provides a mechanism for the intestinal mucosa to efficiently biosynthesize nucleotides and promote energy balance, with this work identifying exogenous purines as critical substrates for the proliferative wound healing response.

Goblet cells substantially benefit from the nucleotides and energy derived from MSPs, in accordance with their high demand to synthesize and secrete large amounts of mucin proteins. The need for nucleotides in the protein-synthesizing process is most prominent during transcription, after which the translation of secretory proteins on the ER is driven by GTP hydrolysis. From there, numerous processes such as protein translocation, folding, post-translational modifications, and trafficking require ATP (Depaoli et al., 2019). Without sufficient GTP and ATP supply, the ER becomes stressed and protein construction stalls, rendering the cell unable to yield properly folded and packaged mucin for secretion. Consequently, the sterile integrity of the colonic inner mucin layer upon injury is dependent on purine supply, presenting an interesting evolutionary corollary of this MSP-host relationship, in which the stimulation of mucin secretion by MSPs may subserve a symbiotic feedback loop between the colonic epithelia and microbiota, where the microbiota supplies the purine necessary for mucous generation as a microbial habitat and fuel source.

In addition to their many intracellular roles, purines are known to function as extracellular signaling molecules. For instance, activated polymorphonuclear leukocytes (PMNs) and platelets release large amounts of ATP during the transmigration process (Eltzschig et al., 2003; Weissmuller et al., 2008). ATP (or ADP) is rapidly metabolized to AMP by the membrane-bound enzyme ectonucleoside triphosphate

diphosphohydolase 1 (CD39) and subsequentially into adenosine (Ado) by ecto-5′-nucleotidase (CD73), at which point Ado signals through one or more of four transmembrane G protein-coupled receptors (A1, A2A, A2B, and A3) to drive anti-inflammatory and pro-barrier responses (Aherne et al., 2015, 2018; Eltzschig et al., 2006). Although Ado signaling ends upon intracellular incorporation of the purine via equilibrative nucleotide transporters, notably ENT1 and ENT2 (Eckle et al., 2013; Eltzschig et al., 2005; Griffiths et al., 1997), this transport of Ado across the cellular membrane marks the beginning of Ado salvage. Recent purine analyses of cultured T84 IECs and murine colon tissue extracts revealed relatively low Ado levels in general (Lee et al., 2018), suggesting that intracellular Ado is quickly metabolized, perhaps in an effort to minimize [Ado] to limit the inhibition of pyrimidine biosynthesis and ultimately proliferation (Hershfield et al., 1977; Ishii and Green, 1973; Marcelino et al., 2019). Interestingly, hypoxia, such as that associating with mucosal inflammation, represses adenosine kinase activity, leaving adenosine deaminase to metabolize the incorporated Ado into Ino (Morote-Garcia et al., 2008). This influx of Ado and repression of adenosine kinase may account for the Ino increases observed in murine colon tissue subjected to DSS and represents a potential additional mechanism through which PMNs promote mucosal healing by supplying purine substrate for proliferation (Figure S1).

Shifts in the metabolism and composition of the colonic microbiota (dysbiosis) might underlie a number of human diseases through mechanisms that remain elusive. A dysbiosis-induced attenuation of MSPs and ensuing defective mucous production may play a role in promoting colonic inflammation. This dependency on purine supply for mucous generation is of notable therapeutic significance for the treatment of ulcerative colitis (UC). A defective inner mucous layer due to a lack of mucin production, leading to increased contact between the microbiota and mucosa, is a hallmark of and implicated in the pathogenesis of UC (Swidsinski et al., 2007; Ungaro et al., 2017). This implication is exemplified by mice deficient in MUC2 spontaneously developing severe colitis and even inflammation-associated cancer, a result analogous to human patients with UC (Van der Sluis et al., 2006; Velcich et al., 2002). In this, a subset of patients is thought to be afflicted by UC as a consequence of a permeable inner mucous layer rather than a hyperactive immune system (Johansson et al., 2013). Furthermore, the proportion of apoptotic colonic epithelial cells is elevated in patients with UC (Iwamoto et al., 1996; Strater et al., 1997), representing another potential contribution of dysbiotic MSP depletion to disease pathogenesis and continuance. The results of this work suggest that reconstitution or augmentation of MSPs in patients with IBD may provide the energy and substrates needed to promote wound healing and barrier reformation, representing a unique therapeutic approach to promote the remission of inflammatory disorders and wound healing in the gut.

Limitations of the Study

One limitation of the study was the use of streptomycin to deplete the murine colonic mucosa of MSPs. In this regard, streptomycin was used as a tool to accommodate reconstitution by oral Hpx supplementation or by colonization with streptomycin-resistant, purine-producing bacteria. Streptomycin potentially complicated some interpretation of the experimental DSS challenge in cohorts of mice, where streptomycin treatment itself was found to limit disease severity. As infiltration of opportunistic commensal bacteria is a fundamental tenant of disease pathogenesis in DSS colitis, and streptomycin alters the composition of the microbiota, it is reasonable that the protection against disease severity stems from limiting the infiltration of opportunistic bacteria. As a result, care should be taken in comparing the control and streptomycin-treated mouse groups, as the colonic tissues between the groups may be experiencing different mechanisms of disease pathogenesis. Despite this, it is notable that the gut mucosa utilizes and substantially benefits from the nucleotide biosynthetic capacity afforded by the salvage of exogenous purine in both disease settings.

Resource Availability

Lead Contact

Further information and requests for resources should be directed to and will be fulfilled by the Lead Contact, Sean Colgan (sean.colgan@ucdenver.edu).

Materials Availability

The streptomycin-resistant E. coli K12 strain generated for this work is available upon request.

Data and Code Availability

No custom code, software, or algorithms were used, or datasets generated (e.g. microarray) in this work.

METHODS

All methods can be found in the accompanying Transparent Methods supplemental file.

SUPPLEMENTAL INFORMATION

Supplemental Information can be found online at https://doi.org/10.1016/j.isci.2020.101226.

ACKNOWLEDGMENTS

This work was supported by NIH grants F32 DK122741, DK1047893, DK50189, DK095491, and DK103712 and by the Veterans Administration Merit Award BX002182.

AUTHOR CONTRIBUTIONS

Conceptualization, J.S.L. and S.P.C.; Methodology, J.S.L., D.J.K., and S.P.C.; Formal Analysis, J.S.L.; Investigation, J.S.L, R.X.W., M.S.G., and G.P.C.; Resources, S.P.C.; Writing – Original Draft, J.S.L., D.J.K., and S.P.C.; Writing – Review & Editing, J.S.L., R.X.W., and S.P.C.; Visualization, J.S.L.; Funding Acquisition, J.S.L. and S.P.C.

DECLARATION OF INTERESTS

Parts of the work reported herein were used to file a patent application.

Received: March 19, 2020
Revised: May 4, 2020
Accepted: May 29, 2020
Published: June 26, 2020

REFERENCES

Aherne, C.M., Collins, C.B., Rapp, C.R., Olli, K.E., Perrenoud, L., Jedlicka, P., Bowser, J.L., Mills, T.W., Karmouty-Quintana, H., and Blackburn, M.R. (2018). Coordination of ENT2-dependent adenosine transport and signaling dampens mucosal inflammation. JCI Insight *3*, e121521.

Aherne, C.M., Saeedi, B., Collins, C.B., Masterson, J.C., McNamee, E.N., Perrenoud, L., Rapp, C.R., Curtis, V.F., Bayless, A., and Fletcher, A. (2015). Epithelial-specific A2B adenosine receptor signaling protects the colonic epithelial barrier during acute colitis. Mucosal Immunol. *8*, 1324–1338.

Artis, D. (2008). Epithelial-cell recognition of commensal bacteria and maintenance of immune homeostasis in the gut. Nat. Rev. Immunol. *8*, 411.

Atkinson, D.E. (1977). 4 - adenylate control and the adenylate energy charge. In Cellular Energy Metabolism and its Regulation (Academic Press), pp. 85–107.

Atkinson, D.E., and Walton, G.M. (1967). Adenosine triphosphate conservation in metabolic regulation rat liver citrate cleavage enzyme. J. Biol. Chem. *242*, 3239–3241.

Depaoli, M.R., Hay, J.C., Graier, W.F., and Malli, R. (2019). The enigmatic ATP supply of the endoplasmic reticulum. Biol. Rev. *94*, 610–628.

Eckburg, P.B., Bik, E.M., Bernstein, C.N., Purdom, E., Dethlefsen, L., Sargent, M., Gill, S.R., Nelson, K.E., and Relman, D.A. (2005). Diversity of the human intestinal microbial flora. Science *308*, 1635–1638.

Eckle, T., Hughes, K., Ehrentraut, H., Brodsky, K.S., Rosenberger, P., Choi, D.-S., Ravid, K., Weng, T., Xia, Y., and Blackburn, M.R. (2013). Crosstalk between the equilibrative nucleoside transporter ENT2 and alveolar Adora2b adenosine receptors dampens acute lung injury. FASEB J. *27*, 3078–3089.

Eltzschig, H.K., Abdulla, P., Hoffman, E., Hamilton, K.E., Daniels, D., Schönfeld, C., Löffler, M., Reyes, G., Duszenko, M., and Karhausen, J. (2005). HIF-1–dependent repression of equilibrative nucleoside transporter (ENT) in hypoxia. J. Exp. Med. *202*, 1493–1505.

Eltzschig, H.K., Ibla, J.C., Furuta, G.T., Leonard, M.O., Jacobson, K.A., Enjyoji, K., Robson, S.C., and Colgan, S.P. (2003). Coordinated adenine nucleotide phosphohydrolysis and nucleoside signaling in posthypoxic endothelium: role of ectonucleotidases and adenosine A_{2B} receptors. J. Ex Med. *198*, 783–796.

Eltzschig, H.K., Weissmüller, T., Mager, A., and Eckle, T. (2006). Nucleotide metabolism and cell-cell interactions. In Cell-Cell Interactions, Sean Colgan, ed. (Springer), pp. 73–87.

Garcia, D., and Shaw, R.J. (2017). AMPK: mechanisms of cellular energy sensing and restoration of metabolic balance. Mol. Cell *66*, 789–800.

Griffiths, M., Beaumont, N., Yao, S.Y.M., Sundaram, M., Boumah, C.E., Davies, A., Kwong, F.Y.P., Coe, I., Cass, C.E., and Young, J.D. (1997). Cloning of a human nucleoside transporter implicated in the cellular uptake of adenosine and chemotherapeutic drugs. Nat. Med. *3*, 89–93.

Grimble, G.K. (1994). Dietary nucleotides and gut mucosal defence. Gut *35*, S46–S51.

Groschwitz, K.R., and Hogan, S.P. (2009). Intestinal barrier function: molecular regulation and disease pathogenesis. J. Allergy Clin. Immunol. *124*, 3–20.

Hardie, D.G. (2014). AMPK—sensing energy while talking to other signaling pathways. Cell Metab. *20*, 939–952.

Hardie, D.G., Ross, F.A., and Hawley, S.A. (2012). AMPK: a nutrient and energy sensor that maintains energy homeostasis. Nat. Rev. Mol. Cell Biol. *13*, 251.

Hartsock, A., and Nelson, W.J. (2008). Adherens and tight junctions: structure, function and connections to the actin cytoskeleton. Biochim. Biophys. Acta *1778*, 660–669.

Hershfield, M.S., Snyder, F.F., and Seegmiller, J.E. (1977). Adenine and adenosine are toxic to human lymphoblast mutants defective in purine salvage enzymes. Science *197*, 1284–1287.

Hetz, C., and Papa, F.R. (2018). The unfolded protein response and cell fate control. Mol. Cell *69*, 169–181.

Hirokawa, N., Keller, T.C., 3rd, Chasan, R., and Mooseker, M.S. (1983). Mechanism of brush border contractility studied by the quick-freeze, deep-etch method. J. Cell Biol. *96*, 1325–1336.

Hooper, L.V., and Macpherson, A.J. (2010). Immune adaptations that maintain homeostasis with the intestinal microbiota. Nat. Rev. Immunol. *10*, 159.

Hoxhaj, G., Hughes-Hallett, J., Timson, R.C., Ilagan, E., Yuan, M., Asara, J.M., Ben-Sahra, I., and Manning, B.D. (2017). The mTORC1 signaling

network senses changes in cellular purine nucleotide levels. Cell Rep. *21*, 1331–1346.

Ishii, K., and Green, H. (1973). Lethality of adenosine for cultured mammalian cells by interference with pyrimidine biosynthesis. J. Cell Sci. *13*, 429–439.

Ivanov, A.I., Parkos, C.A., and Nusrat, A. (2010). Cytoskeletal regulation of epithelial barrier function during inflammation. Am. J. Pathol. *177*, 512–524.

Iwahana, H., Honda, S., Tsujisawa, T., Takahashi, Y., Adzuma, K., Katashima, R., Yamaoka, T., Moritani, M., Yoshimoto, K., and Itakura, M. (1995). Rat genomic structure of amidophosphoribosyltransferase, cDNA sequence of aminoimidazole ribonucleotide carboxylase, and cell cycle-dependent expression of these two physically linked genes. Biochim. Biophys. Acta *1261*, 369–380.

Iwamoto, M., Koji, T., Makiyama, K., Kobayashi, N., and Nakane, P.K. (1996). Apoptosis of crypt epithelial cells in ulcerative colitis. J. Pathol. *180*, 152–159.

Javitt, G., Calvo, M.L.G., Albert, L., Reznik, N., Ilani, T., Diskin, R., and Fass, D. (2019). Intestinal gel-forming mucins polymerize by disulfide-mediated dimerization of d3 domains. J. Mol. Biol. *431*, 3740–3752.

Johansson, M.E.V., Gustafsson, J.K., Sjöberg, K.E., Petersson, J., Holm, L., Sjövall, H., and Hansson, G.C. (2010). Bacteria penetrate the inner mucus layer before inflammation in the dextran sulfate colitis model. PLoS One *5*, e12238.

Johansson, M.E.V., Phillipson, M., Petersson, J., Velcich, A., Holm, L., and Hansson, G.C. (2008). The inner of the two Muc2 mucin-dependent mucus layers in colon is devoid of bacteria. Proc. Natl. Acad. Sci. U S A *105*, 15064–15069.

Johansson, M.E.V., Sjövall, H., and Hansson, G.C. (2013). The gastrointestinal mucus system in health and disease. Nat. Rev. Gastroenterol. Hepatol. *10*, 352.

Juelicher, F., Kruse, K., Prost, J., and Joanny, J.F. (2007). Active behavior of the cytoskeleton. Phys. Rep. *449*, 3–28.

Kaser, A., Zeissig, S., and Blumberg, R.S. (2010). Inflammatory bowel disease. Annu. Rev. Immunol. *28*, 573–621.

Kazimieras Malys, M., Campbell, L., and Malys, N. (2015). Symbiotic and antibiotic interactions between gut commensal microbiota and host immune system. Medicina *51*, 69–75.

Kelly, C.J., Zheng, L., Campbell, E.L., Saeedi, B., Scholz, C.C., Bayless, A.J., Wilson, K.E., Glover, L.E., Kominsky, D.J., and Magnuson, A. (2015). Crosstalk between microbiota-derived short-chain fatty acids and intestinal epithelial HIF augments tissue barrier function. Cell Host Microbe *17*, 662–671.

Kim, M.H., Kang, S.G., Park, J.H., Yanagisawa, M., and Kim, C.H. (2013). Short-chain fatty acids activate GPR41 and GPR43 on intestinal epithelial cells to promote inflammatory responses in mice. Gastroenterology *145*, 396–406.

Lane, A.N., and Fan, T.W.M. (2015). Regulation of mammalian nucleotide metabolism and biosynthesis. Nucleic Acids Res. *43*, 2466–2485.

Laukoetter, M.G., Nava, P., and Nusrat, A. (2008). Role of the intestinal barrier in inflammatory bowel disease. World J. Gastroenterol. *14*, 401.

Lee, J.S., Wang, R.X., Alexeev, E.E., Lanis, J.M., Battista, K.D., Glover, L.E., and Colgan, S.P. (2018). Hypoxanthine is a checkpoint stress metabolite in colonic epithelial energy modulation and barrier function. J. Biol. Chem. *293*, 6039–6051.

LeLeiko, N.S., Bronstein, A.D., Baliga, B.S., and Munro, H.N. (1983). De novo purine nucleotide synthesis in the rat small and large intestine: effect of dietary protein and purines. J. Pediatr. Gastroenterol. Nutr. *2*, 313–319.

Ley, R.E., Bäckhed, F., Turnbaugh, P., Lozupone, C.A., Knight, R.D., and Gordon, J.I. (2005). Obesity alters gut microbial ecology. Proc. Natl. Acad. Sci. U S A *102*, 11070–11075.

Macia, L., Tan, J., Vieira, A.T., Leach, K., Stanley, D., Luong, S., Maruya, M., McKenzie, C.I., Hijikata, A., and Wong, C. (2015). Metabolite-sensing receptors GPR43 and GPR109A facilitate dietary fibre-induced gut homeostasis through regulation of the inflammasome. Nat. Commun. *6*, 6734.

Mackinnon, A.M., and Deller, D.J. (1973). Purine nucleotide biosynthesis in gastrointestinal mucosa. Biochim. Biophys. Acta *319*, 1–4.

Maloy, K.J., and Powrie, F. (2011). Intestinal homeostasis and its breakdown in inflammatory bowel disease. Nature *474*, 298.

Marcelino, H., Nogueira, V.C., Santos, C.R.A., Quelhas, P., Carvalho, T.M.A., Fonseca-Gomes, J., Tomás, J., Diógenes, M.J., Sebastião, A.M., and Cascalheira, J.F. (2019). Adenosine inhibits human astrocyte proliferation independently of adenosine receptor activation. J. Neurochem. *153*, e14937.

Meddings, J.B. (1997). Intestinal permeability in Crohn's disease. Aliment. Pharmacol. Ther. *11*, 47–56.

Morote-Garcia, J.C., Rosenberger, P., Kuhlicke, J., and Eltzschig, H.K. (2008). HIF-1–dependent repression of adenosine kinase attenuates hypoxia-induced vascular leak. Blood *111*, 5571–5580.

Natsumeda, Y., Prajda, N., Donohue, J.P., Glover, J.L., and Weber, G. (1984). Enzymic capacities of purine de novo and salvage pathways for nucleotide synthesis in normal and neoplastic tissues. Cancer Res. *44*, 2475–2479.

Nicholson, J.K., Holmes, E., Kinross, J., Burcelin, R., Gibson, G., Jia, W., and Pettersson, S. (2012). Host-gut microbiota metabolic interactions. Science *336*, 1262–1267.

Nicholson, J.K., and Wilson, I.D. (2003). Understanding'global'systems biology: metabonomics and the continuum of metabolism. Nat. Rev. Drug Discov. *2*, 668–676.

Okumura, R., and Takeda, K. (2017). Roles of intestinal epithelial cells in the maintenance of gut homeostasis. Exp. Mol. Med. *49*, e338.

Pareek, V., Tian, H., Winograd, N., and Benkovic, S.J. (2020). Metabolomics and mass spectrometry imaging reveal channeled de novo purine synthesis in cells. Science *368*, 283–290.

Pelaseyed, T., Bergström, J.H., Gustafsson, J.K., Ermund, A., Birchenough, G.M.H., Schütte, A., van der Post, S., Svensson, F., Rodríguez-Piñeiro, A.M., and Nyström, E.E.L. (2014). The mucus and mucins of the goblet cells and enterocytes provide the first defense line of the gastrointestinal tract and interact with the immune system. Immunological Rev. *260*, 8–20.

Rao, R.V., and Bredesen, D.E. (2004). Misfolded proteins, endoplasmic reticulum stress and neurodegeneration. Curr. Opin. Cell Biol. *16*, 653–662.

Savaiano, D.A., and Clifford, A.J. (1981). Adenine, the precursor of nucleic acids in intestinal cells unable to synthesize purines de novo. J. Nutr. *111*, 1816–1822.

Schilderink, R., Verseijden, C., Seppen, J., Muncan, V., Van Den Brink, G.R., Lambers, T.T., van Tol, E.A., and de Jonge, W.J. (2016). The SCFA butyrate stimulates the epithelial production of retinoic acid via inhibition of epithelial HDAC. Am. J. Physiol. *310*, G1138–G1146.

Schmitz, H., Barmeyer, C., Fromm, M., Runkel, N., Foss, H.-D., Bentzel, C.J., Riecken, E.-O., and Schulzke, J.-D. (1999). Altered tight junction structure contributes to the impaired epithelial barrier function in ulcerative colitis. Gastroenterology *116*, 301–309.

Sekirov, I., Tam, N.M., Jogova, M., Robertson, M.L., Li, Y., Lupp, C., and Finlay, B.B. (2008). Antibiotic-induced perturbations of the intestinal microbiota alter host susceptibility to enteric infection. Infect. Immun. *76*, 4726–4736.

Smith, J.L. (1998). Glutamine PRPP amidotransferase: snapshots of an enzyme in action. Curr. Opin. Struct. Biol. *8*, 686–694.

Strater, J., Wellisch, I., Riedl, S., Walczak, H., Koretz, K., Tandara, A., Krammer, P.H., and Moller, P. (1997). CD95 (APO-1/Fas)-mediated apoptosis in colon epithelial cells: a possible role in ulcerative colitis. Gastroenterology *113*, 160–167.

Suzuki, T. (2013). Regulation of intestinal epithelial permeability by tight junctions. Cell Mol. Life Sci. *70*, 631–659.

Swidsinski, A., Loening-Baucke, V., Theissig, F., Engelhardt, H., Bengmark, S., Koch, S., Lochs, H., and Dörffel, Y. (2007). Comparative study of the intestinal mucus barrier in normal and inflamed colon. Gut *56*, 343–350.

Tan, J., McKenzie, C., Potamitis, M., Thorburn, A.N., Mackay, C.R., and Macia, L. (2014). The role of short-chain fatty acids in health and disease. Adv. Immunol. *121*, 91–119.

Taylor, C.T., and Colgan, S.P. (2017). Regulation of immunity and inflammation by hypoxia in immunological niches. Nat. Rev. Immunol. *17*, 774–785.

Ungaro, R., Mehandru, S., Allen, P.B., Peyrin-Biroulet, L., and Colombel, J.-F. (2017). Ulcerative colitis. Lancet *389*, 1756–1770.

Ursell, L.K., Haiser, H.J., Van Treuren, W., Garg, N., Reddivari, L., Vanamala, J., Dorrestein, P.C., Turnbaugh, P.J., and Knight, R. (2014). The intestinal metabolome: an intersection between microbiota and host. Gastroenterology *146*, 1470–1476.

Van der Sluis, M., De Koning, B.A.E., De Bruijn, A.C.J.M., Velcich, A., Meijerink, J.P.P., Van Goudoever, J.B., Büller, H.A., Dekker, J., Van Seuningen, I., and Renes, I.B. (2006). Muc2-deficient mice spontaneously develop colitis, indicating that MUC2 is critical for colonic protection. Gastroenterology *131*, 117–129.

Velcich, A., Yang, W., Heyer, J., Fragale, A., Nicholas, C., Viani, S., Kucherlapati, R., Lipkin, M., Yang, K., and Augenlicht, L. (2002). Colorectal cancer in mice genetically deficient in the mucin Muc2. Science *295*, 1726–1729.

Weber, G., Jayaram, H.N., Pillwein, K., Natsumeda, Y., Reardon, M.A., and Zhen, Y.-S. (1987). Salvage pathways as targets of chemotherapy. Adv. Enzyme Regul. *26*, 335–352.

Weber, G., Lui, M.S., Natsumeda, Y., and Faderan, M.A. (1983). Salvage capacity of hepatoma 3924A and action of dipyridamole. Adv. Enzyme Regul. *21*, 53–69.

Weissmuller, T., Campbell, E.L., Rosenberger, P., Scully, M., Beck, P.L., Furuta, G.T., and Colgan, S.P. (2008). PMNs facilitate translocation of platelets across human and mouse epithelium and together alter fluid homeostasis via epithelial cell-expressed ecto-NTPDases. J. Clin. Invest. *118*, 3682–3692.

Yamaoka, T., Kondo, M., Honda, S., Iwahana, H., Moritani, M., Ii, S., Yoshimoto, K., and Itakura, M. (1997). Amidophosphoribosyltransferase limits the rate of cell growth-linked de novo purine biosynthesis in the presence of constant capacity of salvage purine biosynthesis. J. Biol. Chem. *272*, 17719–17725.

Zhu, J., and Thompson, C.B. (2019). Metabolic regulation of cell growth and proliferation. Nat. Rev. Mol. Cell Biol. *20*, 436–450.

iScience, Volume *23*

Supplemental Information

Microbiota-Sourced Purines Support Wound Healing and Mucous Barrier Function

J. Scott Lee, Ruth X. Wang, Matthew S. Goldberg, Garrett P. Clifford, Daniel J. Kao, and Sean P. Colgan

SUPPLEMENTAL FIGURE

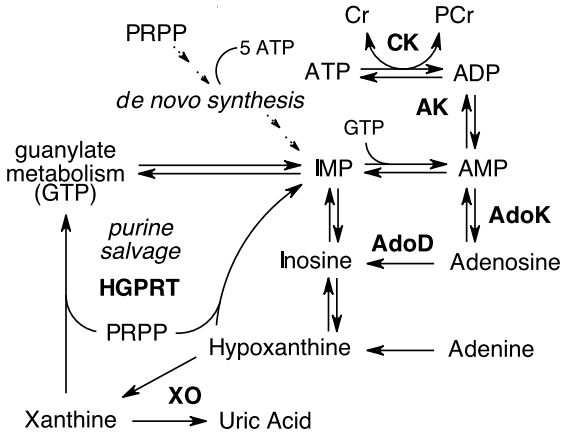

Figure S1. Related to Figures 1F and 2G. The purine metabolic pathway.

Graphical summary of the purine metabolic pathway. IMP, inosine monophosphate; AMP, adenosine monophosphate; ADP, adenosine diphosphate; ATP, adenosine triphosphate; Cr, creatine; PCr, phosphocreatine; PRPP, phosphoribosyl pyrophosphate; GTP, guanosine triphosphate; XO, xanthine oxidase; HGPRT, hypoxanthine-guanine phosphoribosyltransferase; AK, adenylate kinase; CK, creatine kinase; AdoK, adenosine kinase; AdoD, adenosine deaminase.

TRANSPARENT METHODS

Key Resources Table

REAGENT or RESOURCE	SOURCE	IDENTIFIER
Antibodies		
Ki-67 Monoclonal	Thermo Fisher Scientific	Cat#14-5698-82; RRID: AB_10854564
BiP/GRP78/HSPA5	Novus Biologicals	Cat#NBP1-06277; RRID: AB_1556186
E. coli	Novus Biologicals	Cat#NB200-579; RRID: AB_10002133
Goat anti-Rabbit IgG (H+L) Highly Cross-Adsorbed Secondary Antibody, Alexa Fluor 488	Thermo Fisher Scientific	Cat#A-11034; AB_2576217
Goat anti-Rat IgG (H+L) Cross Adsorbed Secondary Antobody, Alex Fluor 555	Thermo Fisher Scientific	Cat#A-21434; RRID: AB_2535855
Chemicals, Peptides, and Recombinant Proteins		
Acetonitrile (HPLC)	Fisher Scientific	Cat#A998; CAS: 75-05-8
Methanol (HPLC)	Fisher Scientific	Cat#A452; CAS: 67-56-1
Methanol, Absolute – Acetone free	Millipore Sigma	Cat#M1775; CAS: 67-56-1
Potassium phosphate monobasic for HPLC, LiChropur	Millipore Sigma	Cat#57618; CAS: 7778-77-0
Tetrabutylammonium bisulfate	Millipore Sigma	Cat#86868; CAS: 32503-27-8
Critical Commercial Assays		
TUNEL Assay Kit – HRP-DAB	Abcam	Cat#ab206386

Experimental Models: Organisms/Strains		
Mouse: C57BL/6J	The Jackson Laboratory	Cat#00664; RRID: IMSR_JAX:000664
Oligonucleotides		
E. coli rpsL mutagenic oligo: G*T*C*A*GACGAACACGGCATACTTTACGCAGCGCG GAGTTCGGTTTTCTAGGAGTGGTAGTATATACACGA GTACATACGCCACGTTTTTGC	This Paper	N/A
Recombinant DNA		
pORTMAGE-3	addgene	Cat#72678; RRID: Addgene_72678
Software and Algorithms		
Prism	GraphPad	https://www.graphpad.com/scientific-software/prism/; RRID: SCR_002798
Agilent OpenLab	Agilent	https://www.agilent.com/en/products/software-informatics/openlab-software-suite#0
Zen2	Zeiss	https://www.zeiss.com/microscopy/us/products/microscope-software/zen.html

Experimental Model Details

Vertebrate Animal Use

The University of Colorado Anschutz Medical Campus (AMC) animal management program is accredited by the American Association for the Accreditation of Laboratory Animal Care (AAALAC) and meets the National Institutes of Health standards as set forth in the Guide for the Care and Use of Laboratory Animals (DHHS Publication No. (NIH) 85-23). The institution also accepts as mandatory the PHS Policy on Human Care and Use of Laboratory Animals by Awardee Institutions and NIH Principles for the Utilization and Care of Vertebrate Animals Used in Testing, Research and Training.

Murine Hypoxanthine Enemas

Male 15 – 16-week-old mice were depleted of purine producing bacteria by administration of streptomycin in the drinking water (5 g/L) for 3 days. Mice were anesthetized using 3% isoflurane by inhalation dispensed from an anesthesia machine and administered 100 μL of sterile phosphate buffered saline (PBS, pH 7.4) as a control or sterile PBS with 1 mM hypoxanthine by enema ~18 and 5 h before sacrifice. A distal piece of colon tissue (~15 mg) was placed in 500 μL of 80% methanol, flash frozen by immersion in liquid nitrogen, and stored at -80 °C until processed for HPLC metabolite analysis.

Murine K12 Colonizations

Bacterial Preparation for Oral Gavage: A glycerol stock of the streptomycin resistant K12 strain used for the colonization experiments was streaked on LB agarose plates containing streptomycin (50 μg/mL) and grown at 37 °C overnight. A single colony was used to inoculate 2 mL of streptomycin containing LB broth, and the culture grown overnight at 37 °C with shaking. A 1.5 mL aliquot of the culture was centrifuged at 3000 g for 5 min to pellet the bacteria, the supernatant removed, and the bacteria then resuspended in 1.5 ml of PBS in preparation for oral gavage.

Germ-free Mouse Monocolonization: Germ-free mice were provided by the University of Colorado AMC gnotobiotic core. Female 7 – 8 week old gnotobiotic mice were administered 100 μL of the K12 bacterial preparation by oral gavage and allowed one week for colonization and complete turnover of the colonic epithelium, as described previously (Alexeev et al., 2018). Mice subjected to dextran sodium sulfate (DSS)-induced colitis were administered 3% DSS in drinking water for 5 days and sacrificed on day 7. K12 colonization was verified before and after DSS treatment by streaking fecal extracts on MacConkey agarose plates containing streptomycin (50 μg/mL) and bacteria grown at 37 °C overnight. A distal segment of colon tissue (~15 mg) was placed in 500 μL of 80% methanol, flash frozen by immersion in liquid nitrogen, and stored at -80 °C until processed for HPLC metabolite analysis. Fecal pellets were also flash frozen and similarly stored until HPLC analysis.

Conventionally raised Mouse Purine Depletion and K12 Reconstitution: Female 8-week-old C57BL/6J mice were ordered from The Jackson Laboratory and adapted to the University of Colorado AMC animal facility for one week. Mice receiving streptomycin were administered the antibiotic in the drinking water (5 g/L), and those being colonized with K12 were done so the next day by administration of 100 μL of the K12 bacterial preparation by oral gavage. All mice were then equilibrated to the treatments for one week to allow for complete turnover of the colonic epithelium. Mice receiving streptomycin were maintained on the antibiotic throughout all experimentation. Mice submitted to dextran sodium sulfate (DSS)-induced colitis were administered 3% DSS in drinking water for 5 days and sacrificed on day 7. K12 colonization was verified before and after DSS treatment by streaking fecal extracts on MacConkey agarose plates containing streptomycin and bacteria grown at 37 °C overnight. A piece of colon tissue encompassing the most distal fecal pellet was excised and fixed in methacarn (60% absolute methanol, 30% chloroform, 10% glacial acetic acid, v/v) for histology, as described previously (Kuhn et al., 2018). A distal piece of colon tissue (~15 mg) was placed in 500 μL of 80% methanol, flash frozen by immersion in liquid nitrogen, and stored at -80 °C until processed for HPLC metabolite analysis.

Method Details

Streptomycin-resistant K12 Preparation

The streptomycin-resistant *rpsL* R86S *E. coli* mutant strain was generated through a single cycle of multiplex automated genome engineering (MAGE) using the pORTMAGE-3 plasmid. pORTMAGE-3 was a gift from Csaba Pál. The BW25113 parent strain was transformed with the pORTMAGE-3 plasmid and MAGE recombineering was performed as described previously (Nyerges et al., 2016). The *E. coli* rpsL mutagenic oligonucleotide was synthesized with four phosphorothioate linkages at the 5′ terminus (Wang et al., 2012). The *rpsL* R86S mutants were selected through plating on LB agar with kanamycin and streptomycin. Curing of the pORTMAGE-3 plasmid was accomplished through growth at 37 °C. Verification that the mutant colonies had lost the pORTMAGE-3 plasmid was performed through replicate plating on single and dual selection LB agar.

HPLC Analyses

Extracellular Fecal Metabolites: Fecal pellets were removed from -80 °C and dispersed in 500 μL of ice-cold Milli-Q (mq) water. All extractions were performed on ice. The sample was vortexed for ~10 s and then centrifuged at 18,000 g and 4 °C for 10 min. The supernatant was then transferred to a new tube, another 500 μL of mq water added to the fecal matter, and the matter resuspended. The extraction process was repeated two more times, producing a total of 1.5 mL of extract. The extract was dried using and Eppendorf Vacufuge at room temperature. The dried extract was dissolved in 400 μL of mobile phase A (details below), filtered through a Vivaspin 5,000 MWCO PES column (Sartorius Stedim Biotech), and submitted to HPLC analysis.

Colon Tissue Metabolites: Colon tissue metabolites extracted as previously described with minor variations (Lee et al., 2018). Approximately ~15 mg of whole, distal colon was quickly placed in 500 μl of 80% MeOH and flash-frozen under liquid nitrogen to quench metabolic activity. The frozen tissue was stored at −80 °C, if necessary, before continuing on with the metabolite extraction procedure. All extractions were performed on ice. For metabolite extraction, the tissue was first sonicated 3 × 10 s (BioLogics Inc., 150 V/T Ultrasonic Homogenizer, power output ~20). The sample was then placed in

liquid nitrogen until frozen, removed and thawed, and vortexed for ~10 s. The sample was centrifuged for 10 min at 18,000 g and 4 °C, and the supernatant transferred to a new Eppendorf tube. Another 500 µl of 80% MeOH was then added to the sample, the tissue resuspended, and the extraction process repeated twice more. The resulting 1.5 ml of extract was dried via an Eppendorf Vacufuge at room temperature. The dried extract was dissolved in 400 µl of mobile phase A (details below) and filtered (Whatman Puradisc 4, 0.45 µm, nylon) into vials for HPLC injection.

HPLC Protocol: Metabolites were analyzed by HPLC as previously described with minor variations (Lee et al., 2018). Analyses were performed on an Agilent Technologies 1260 Infinity HPLC using a Phenomenex Luna 3 µm C18(2) column (100 Å, 150 × 4.6 mm) (mobile phase A, 50 mM KH_2PO_4, 5 mM tetrabutylammonium bisulfate, pH 6.25; mobile phase B, acetonitrile; column temperature, 30 °C; flow rate, 1 ml/min). Chromatographic separation of the metabolites was performed using a combination of isocratic and gradient methods, including column washing and equilibration periods at the end (0 min, 100% A; 7 min, 100% A; 10 min, 97% A; 18 min, 97% A; 45 min, 86% A; 60 min, 50% A; 80 min, 50% A; 90 min, 100% A; 135 min, 100% A). The metabolites were detected by absorption at wavelengths of 210, 254, and 280 nm, with their absorbance spectra and retention times verified by co-injection with authentic standards. Metabolites were quantitated from calibration curves developed from the injection of standards ranging from 100 nM to 5 mM.

Histological Analyses

Paraffin embedding of tissue and slide preparation (blank and H&E) was performed by the University of Colorado AMC Department of Pathology histology laboratory. Slides were deparaffinized through a series of washes: xylene, 2 × 3 min; xylene:ethanol::1:1, 3 min; ethanol, 2 × 3 min; 95% ethanol, 3 min; 70% ethanol, 3 min; 50% ethanol, 3 min; rinse in cold tap water.

Immunofluorescence: Deparaffinized slides were placed in Tris-EDTA buffer (10 mM Tris base, 1 mM EDTA, 0.05% Tween 20, pH 9.0) for heat-induced epitope retrieval (HIER) (Biocare Medical Decloaking Chamber, DC2008US). HIER was performed at 80 °C for 1 h (Ki67) or 125 °C for 30 s (BiP) and the slides then equilibrated to room temperature. The slides were washed 2 × 5 min in TBS wash buffer (50 mM Tris, 150 mM NaCl, 0.025% Triton X-100, pH 7.6), the tissue permeabilized by immersion in TBS wash buffer containing 0.2% Triton X-100 for 8 min, then the slides washed again 2 × 5 min in TBS wash buffer. No HIER or permeabilization was performed for the *E. coli* immunofluorescent analyses, and the washes were performed in TBS only. The tissue was blocked using 10% normal goat serum and 1% bovine serum albumin (BSA) in Tris buffered saline (TBS, 50 mM Tris, 150mM NaCL, pH 7.6) for 2 h at room temperature. No HIER or permeabilization was performed on slides for *E. coli* immunofluorescence, and washes were performed in TBS only. Primary antibody in TBS containing 1% BSA (Ki67, 1:100; BiP, 1:50; *E. coli*, 1:10) was then added to the tissue and the slides incubated overnight at 4 °C. The slides were then washed 2 × 5 min in TBS wash buffer and secondary antibody added (1:500 in 1% BSA TBS) and incubated for 1 h at room temperature. Then the slides were rinsed 3 × 5 min in TBS, a coverslip added using ProLong Diamond Mountant with DAPI, and the slides cured for 24 h. Fluorescent images of the tissue were taken using a Zeiss AxioCam MRc 5 at 100X or 200X magnification. Multiple, non-overlapping images of each tissue section from each mouse group (n = 3 – 5) were taken, and all images used for quantification. Images were processed and quantitated using the Zeiss Zen2 program. Immunofluorescence was quantified by drawing appropriate regions of interest for the target being analyzed and normalized to DAPI (target/DAPI, fluorescence sum/sum).

Mucosal Depth: Measurements (n = 21 - 24) of the mucosa depth were determined from representative images (n = 7 – 8) of the H&E stains that span the tissue sections from each mouse cohort (n = 4 – 5). Images were taken using a Zeiss AxioCam MRc 5 at 200X magnification, and measurements performed using the Zeiss Zen2 program.

TUNEL Staining: An Abcam TUNEL HRP-DAB Assay Kit (ab206386) was purchased and applied to deparaffinized slides obtained from each mouse cohort (n = 4) as per the manufacturer instructions. The slides were dehydrated by soaking in 70%, 95%, and 100% ethanol for 3 min each, cleared in xylenes for 3 min, and then mounted with coverslip using Cytoseal 60. The number of TUNEL positive cells in each colon cross section was counted and divided by the mucosal depth to normalize.

Mucin Staining: Deparaffinized slides were placed in Alcian Blue solution (1% in 3% acetic acid, pH 2.5) for 30 min. The slides were then washed in deionized water for 2 min, counterstained with nuclear fast red for 5 min, and washed for 1 min in deionized water. The slides were dehydrated by soaking in 70%, 95%, and 100% ethanol for 3 min each, cleared in xylenes for 3 min, and then mounted with coverslip using Cytoseal 60. Multiple, non-overlapping images of each tissue section from each mouse group (n = 5) were taken using a Zeiss AxioCam MRc 5 at 100X magnification, as described previously (Campbell et al., 2014).

Inner Mucus Layer Depth Measurements: The sterile, inner mucus region of the epithelia was measured through *E. coli* immunofluorescence analyses on colonic tissue sections, as described in the past (Kuhn et al., 2018). Representative images across each tissue section were taken using a Zeiss AxioCam MRc 5 at 100X magnification from each mouse group (n = 5). Multiple measurements distributed across each image (n = 5) from the surface of the epithelium to the luminal *E. coli* were performed to determine the depth of the inner mucus layer.

Statistical Analyses

Statistical analyses were performed in GraphPad Prism 8 using an unpaired two-tailed parametric t-test for direct comparisons. Statistical differences were considered significant when $p \leq 0.05$.

REFERENCES

Alexeev, E.E., Lanis, J.M., Kao, D.J., Battista, K.D., Campbell, E.L., Kelly, C.J., Gerich, M.E., Jenkins, B.R., Walk, S.T., Kominsky, D.J.*, et al.* (2018). Microbiota-derived indole metabolites promote intestinal homeostasis and serve as biomarkers of human inflammatory bowel disease. Am J Pathol *188*, 6039-6051.

Campbell, E.L., Bruyninckx, W.J., Kelly, C.J., Glover, L.E., McNamee, E.N., Bowers, B.E., Bayless, A.J., Scully, M., Saeedi, B.J., Golden-Mason, L.*, et al.* (2014). Transmigrating neutrophils shape the mucosal microenvironment through localized oxygen depletion to influence resolution of inflammation. Immunity *40*, 66-77.

Kuhn, K.A., Schulz, H.M., Regner, E.H., Severs, E.L., Hendrickson, J.D., Mehta, G., Whitney, A.K., Ir, D., Ohri, N., and Robertson, C.E. (2018). Bacteroidales recruit IL-6-producing intraepithelial lymphocytes in the colon to promote barrier integrity. Mucosal immunology *11*, 357-368.

Lee, J.S., Wang, R.X., Alexeev, E.E., Lanis, J.M., Battista, K.D., Glover, L.E., and Colgan, S.P. (2018). Hypoxanthine is a checkpoint stress metabolite in colonic epithelial energy modulation and barrier function. Journal of Biological Chemistry *293*, 6039-6051.

Nyerges, Á., Csörgő, B., Nagy, I., Bálint, B., Bihari, P., Lázár, V., Apjok, G., Umenhoffer, K., Bogos, B., and Pósfai, G. (2016). A highly precise and portable genome engineering method allows comparison of mutational effects across bacterial species. Proceedings of the National Academy of Sciences *113*, 2502-2507.

Wang, H.H., Kim, H., Cong, L., Jeong, J., Bang, D., and Church, G.M. (2012). Genome-scale promoter engineering by coselection MAGE. Nature methods *9*, 591.